

Low-cost ceramic microfiltration membranes made from Moroccan clay for domestic wastewater and Congo Red dye treatment

Soulaiman Iaich^{a,b,*}, Youssef Miyah^c, Fatima Elazhar^{d,e}, Salek Lagdali^{a,b},
Mohamed El-Habacha^{a,b}

^aResearch Team of Energy and Sustainable Development, Higher School of Technology, Guelmim, University Ibn Zohr, Agadir-Morocco, Tel. +212 699 735 637; emails: s.iaich@uiz.ac.ma (S. Iaich), salek.lagdali1991@gmail.com (S. Lagdali)

^bLaboratory of Applied Chemistry and Environment, Faculty of Sciences, University Ibn Zohr, Agadir-Morocco, email: mohamedelhabacha@gmail.com (M. El Habacha)

^cLaboratory of Materials, Processes, Catalysis, and Environment, University Sidi Mohamed Ben Abdellah, School of Technology, P.O. Box: 2427 Fez, Morocco, email: youssef.miyah@gmail.com

^dLaboratory of Separation Processes, Faculty of Sciences, University Ibn Tofail, Kenitra, 14000, Morocco

^eNational Higher School of Chemistry (NHSC), University Ibn Tofail, P.O. Box: 133, 14000 Kenitra, Morocco, email: azh80ar@yahoo.fr

Received 17 February 2021; Accepted 7 July 2021

ABSTRACT

This work addresses the preparation and characterization of low-cost tubular ceramic microfiltration membranes made from Moroccan natural clay. The microfiltration layers (M10/25PVA, M10, and M12) were prepared by the slip-casting technique of suspension containing the clay powder ($\phi < 63 \mu\text{m}$), polyvinyl alcohol, and water. Thereafter, the membranes were dried and sintered at $900^\circ\text{C}/3 \text{ h}$. Chemical analysis by X-ray fluorescence, specific surface, pore size distribution, X-ray diffraction, Fourier transform infrared spectroscopy, differential thermal analysis and thermogravimetric analysis are the techniques used for analyzing and characterizing of our raw clay. The scanning electron microscopy (SEM) analysis, average pore diameter and chemical resistance of all membranes were investigated. The SEM analysis showed that the prepared membranes surface has a homogeneous structure and without defects. The average pore size of the membranes (based on SEM) is 1.76, 1.21, and $1.31 \mu\text{m}$ for M10/25PVA, M10, and M12, respectively. The chemical resistance of membranes is stable in both acidic and basic media. The membranes were selected for microfiltration of domestic wastewater (DWW) and Congo Red (CR) dye. Throughout all of the microfiltration tests, the pH remains relatively stable. The electrical conductivity and the chemical oxygen demand decrease after 45 and 15 min, respectively for all the studied membranes. For DWW, the suspended particulate matter responsible for turbidity is almost eliminated ($R_t = 99\%$), and the CR colored solution has nearly totally discolored ($R_d = 99\%$). The capital cost of three tested ceramic membranes at different operating conditions was evaluated and estimated to be around 21–23 $\$/\text{m}^2$.

Keywords: Ceramic membranes; Low-cost; Cross-flow microfiltration; Domestic wastewater; Congo Red; Turbidity

* Corresponding author.

1. Introduction

Human, domestic, agricultural, and industrial activities produce all kinds of waste which are transported by the liquid way and consequently engender various kinds of pollution and harmful effect in the receiving medium. In this context, several separation techniques, such as photocatalysis, ion exchange, coagulation–flocculation, and adsorption are used to remove pollutants from their respective aqueous sources, but it has been demonstrated that they are no longer sufficient, they require high investment, they could generate secondary waste that is difficult to eradicate and they are just poorly selective [1,2]. The use of the membrane separation technique has been known as a recent very rapid industrial development. Recently, this technique has been found mainly in the agri-food industry, water treatment, sectors of pharmacy, chemistry, biotechnology, and the environment [3–6]. Microfiltration is a very efficient technology for separating solids and recovering products from all kinds of liquids that do not require filter aids and do not produce solid waste [7–9]. Despite these advantages, using cross-flow microfiltration to remove colloids at the industrial level could encounter many situations, the most notable of which are breakthrough, cake forming, concentration polarization, and the leaching of dissolved organic carbon significant amounts during the process. In addition, it is necessary to flush the system with acids and bases as well as large amounts of ultrapure water before and after use [10].

Widely available around the world, clays have non-identical compositions that rely on localized forming conditions and compose a family of minerals in the silicate class, subclass phyllosilicates, layered silicates with layer thicknesses of around 1 nm [11]. The hydrated phyllosilicates ultra-microscopic structure is characterized by the superposition of sheets composed of tetrahedral or octahedral layers that are placed in the interlayers space [12]. They are classified into families according to the thickness of the layers (0.7–1.4 nm): The kaolinite (0.7 nm) that is resulted from weathering feldspars and used in ceramics and the manufacture of porcelain [13]. The montmorillonite where several layers of water can take place between two sheets leading to the interlayer space that can range from 0.96 nm to complete separation [14] and the illite (1 nm) where particles are mostly described as layers with fixed interlayer potassium [15]; besides, the vermiculite (1.4 nm) where the sheet composition is close to that of talc, and the sepiolite (1 nm) that has a fibrous structure [16].

The fabrication of ceramic membranes using different raw materials such as titania, silica, and alumina has been shown in many works of literature [17–19]. The cost of these membranes is very high due to costly raw materials and the need for a sintering temperature that exceeds 1,300°C [20]. Membranes made from the above expensive raw materials are not appropriate for industrial applications from an economic standpoint. To address these issues, researchers are currently looking at other low-cost raw materials that could be used as a conventional raw material substitute. Various clay such as Moroccan clay, Cameroonian clay, Tunisian clay, apatite powder, dolomite, bentonite, and kaolin clay has recently been listed as the most cost-effective raw materials for membrane applications [21–25]. Several researchers

have been working on Moroccan clay and its applications in the field of industrial wastewater treatment and textile dyes because it contains toxic components, potentially carcinogenic for certain organisms [26–29]. It is, therefore, very useful to try to provide economic solutions to clean up and ensure the well-being of our ecosystem. Some researchers, in the field of wastewater treatment, have proven the efficiency of ceramic materials during microfiltration: Bhattacharya et al. [30] conducted a research study that assesses the efficiency of using a ceramic microfiltration process alone and in combination with a biosorbent prepared from fruit peels of *Lagerstroemia speciosa* (L.) Pers for the treatment of industrial and domestic wastewaters. Bouazizi et al. [31] elaborated a Moroccan bentonite ceramic microfiltration membrane to treat tannery and textile effluents while Majouli et al. [32] applied a Moroccan perlite ceramic microfiltration membrane to treat tannery beam house, textile, and electronic industries dicing wafer effluents. Foorginezhad et al. [33] prepared and characterized nano-clay membranes for the microfiltration of cationic dyes. Belgada et al. [34] used a low-cost ceramic microfiltration membrane which was made from natural Moroccan phosphate for pretreatment of raw seawater for desalination.

In the present study, we have made an in-depth physicochemical characterization of our clay, considered as the basic raw material for the manufacture of ceramic microfiltration membranes. For this reason, several experimental characterization techniques were used namely: the X-ray fluorescence chemical analysis (XRF), the measurement of the specific surface and the pore size distribution (BET-PSD), the X-ray diffraction (XRD), the Fourier transform infrared spectroscopy (FTIR), the differential thermal analysis (DTA) and the thermogravimetric analysis (TGA). These techniques allow monitoring the evolution of the material's crystalline phases during heat treatment.

This article aims to develop new ceramic membranes by the slip-casting technique based on raw Moroccan clay while adding on some membranes the polyvinyl alcohol (PVA; M10, M12, and M10/25PVA). The obtained membranes were characterized by the scanning electron microscopy analysis (SEM), average pore diameter and chemical resistance. Moreover, this work is based on the treatment of raw domestic wastewater (DWW) and the Congo Red (CR) anionic dye, which are given their high stability in aqueous media. Therefore, the difficulty of their elimination, as an effective and promising method, is cross-flow microfiltration while studying its influence on the physicochemical parameters of effluents and the ecological and economic aspects of the technological process. The efficiency produced membranes were investigated in terms of permeate flux, pH, electrical conductivity, chemical oxygen demand (COD), turbidity, suspended particulate matter (SPM), as well as the discoloration rate efficiency of CR dye. The study, also, investigated the cost analysis of fabricated ceramic membranes based on the price of raw materials.

2. Materials and methods

2.1. Materials used

The clay we used in this study was taken from the Meknes region located in the North-West of Morocco

(X: 33° 53'42"N; Y: 5° 33'17"W). The wood powder used as a porosity agent in the preparation of our porous ceramic supports comes from solid waste from wood-working. The PVA (Rhodoviol 25/140, Prolabo) used as an organic binder in the preparation of our membranes' layers is a chemical compound with the molecular formula of $(C_2H_4O)_n$ with a repeating unit molecular weight of 44.0526 g/mol. Congo Red (CR, Merck KGaA) is both an organic dye and a pH indicator that is no longer used much due to its toxicity. The CR used is a heterocyclic aromatic chemical compound that has a molecular formula of $(C_{32}H_{22}N_6Na_2O_6S_2)$. It has a molecular weight of 696.66 g/mol. Table 1 shows the chemical structure and characteristics of the CR. Chemical resistance tests were carried out using the nitric acid (HNO_3 , 65 wt.%) and sodium hydroxide (NaOH, 98 wt. %), all of which were obtained from Merck KGaA. Distilled water is also used for all preparations.

2.2. Physicochemical characterization of clay and ceramic membranes

Different techniques were used to characterize the clay. The chemical analysis (XRF) is used by a SIEMENS 300 device. The pore size distribution and the specific surface area of the raw clay were determined by nitrogen adsorption-desorption at 77 K (BET-PSD method-Micromeritics, ASAP 2010). The mineralogy of the clay (raw and heat-treated at 1,000°C/2 h) was determined by the XRD using a SHIMADZU 6100 diffractometer with Cu $K\alpha$ radiation source ($\lambda = 1.54056 \text{ \AA}$) and a Ni filter. A FTIR spectrophotometer (BRUKER VERTEX 70) was used to investigate the molecular characteristics of clay (raw and heat-treated at 1,000°C/2 h). The DTA and the TGA were carried out under a nitrogen atmosphere with a heating rate of 10°C/min, from 25°C to 1,000°C, $\alpha-Al_2O_3$ as reference. The curves were recorded on the thermal analysis apparatus, a type of LABSYS evo TGA, DTA, DSC, and TGA-DTA, TGA-DSC, simultaneous from ambient to 1,600°C. The surface of the microfiltration membranes was characterized in terms of morphology and EDX analysis using an FEI QUANTA 200 SEM. The average pore diameter (d_{ave} , μm) of the ceramic microfiltration membranes was calculated from the SEM images of the membranes of different selected areas using an Image J software (Version 1.4) and the average pore

size was calculated using the below equation considering cylindrical pores [Eq. (1)] [35]:

$$d_{ave} (\mu\text{m}) = \left[\frac{\sum_{i=1}^n n_i d_i^2}{\sum_{i=1}^n n_i} \right]^{0.5} \quad (1)$$

where n refers to the number of pores considered and d_i is the pore diameter (μm) of the i th pore. Chemical stability of the ceramic membranes towards harsh environmental conditions was evaluated by testing the stability of the membranes in acidic and basic conditions through subjecting it to concentrated HNO_3 and NaOH solution for 24 consecutive hours and the results were analyzed by calculating the weight losses (W_L , %) in these conditions [Eq. (2)]:

$$W_L (\%) = \frac{(m_0 - m_1)}{m_0} \times 100 \quad (2)$$

where m_0 is the mass of the sample before chemical contact (g) and m_1 is the mass of the sample after chemical contact (g).

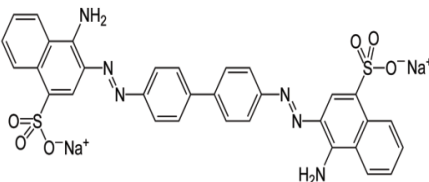
2.3. Analytical methods for characterizing wastewater

Different physicochemical analysis techniques were used for the characterization of wastewater and filtrates obtained by the cross-flow microfiltration process namely: the pH, the electrical conductivity, and the COD were measured using a multiparametric instrument HACH Q430d. The turbidity measurement was determined by a portable turbidimeter of the HACH 2100Q. Furthermore, the turbidity removal efficiency of permeates from DWW (R_t , %) is calculated using the following classical equation [Eq. (3)] [36]:

$$R_t (\%) = \left(1 - \frac{NTU_p}{NTU_f} \right) \times 100 \quad (3)$$

where NTU_p and NTU_f are the turbidity of DWW in permeate and feed, respectively. The SPM is determined by filtration

Table 1
Congo Red dye characteristics

Dye name	Chemical structure	Molar mass (g/mol)	Class	Solubility (g/L)
Congo Red		696.66 ± 0.04	Anionic	Ethanol: 1 Water: 40

through membranes with a pore diameter of 0.45 μm [37]. The difference mass ratio of the filtered water volume gives the concentration of SPM in mg/L [Eq. (4)]:

$$\text{SPM}(\text{mg/L}) = \frac{(M_1 - M_0)}{V_w} \quad (4)$$

where M_0 is the empty membrane mass (mg), M_1 is the mass of membrane and the residues after drying in an oven at 105°C/24 h (mg) and V_w is the filtered water volume (L). The CR discoloration (R_d , %) of each membrane permeates is calculated using the following classical equation [Eq. (5)] [36]:

$$R_d(\%) = \left(1 - \frac{C_p}{C_f}\right) \times 100 \quad (5)$$

where C_f is the concentration of CR in the feed (g/L) and C_p is the concentration of CR in the permeate (g/L). The CR concentrations after microfiltration are determined by an Ultra-Violet spectrophotometry of the type SHIMADZU UV-1800.

2.4. Ceramic membranes preparation

A ceramic paste with ideal characteristics (plasticity, hardness, cohesion, and homogeneity) for extrusion is prepared by mixing the clay powder (0–400 μm) with organic additions (wood powder) and water, the proportions of which are well defined in previous work [38]. The dough is then put in a closed plastic bag and stored in a fridge at constant temperature for a time called aging time (>72 h) to reach homogeneity and to improve the quality of paste by organic additives and water migration. After the aging

step, the dough is then extruded to form single-channel tubular supports. After drying in the open air, the substrates are treated in an electric oven at 1,000°C/3 h for consolidation according to a well-defined thermal program (Fig. 1). The characteristics of the supports used for membranes' layers deposits are given in Table 2.

Then, the microfiltration layers were deposited on the internal surface of the clay support by slip-casting. This technique consists of depositing a stable suspension on the internal face of the support. This suspension called barbotine and is prepared from mineral matter in water. The supports and the microfiltration membranes' layers are made from the same clay. The particle size of the clay powder used to prepare the barbotine (suspension) is less than 63 μm . It must meet a certain number of criteria for it to be usable in the deposit, such as its viscosity, which must be adapted to the use, its homogeneity and its stability to avoid the appearance of undesirable phenomena such as flocculation. Thus, it is necessary to prepare a suitable suspension to use organic additives such as binder PVA. The quantities introduced into the suspension are optimized to obtain, after drying and heat treatment, a reproducible

Table 2
Characteristics of the obtained supports [39]

Geometry support	Single-channel (tubular)
Outside diameter – internal diameter (mm)	24–18
Thickness (mm)	3
Length after sintering (cm)	17
Porosity (%)	36
Mechanical resistance (MPa)	1.98
Filtering surface (cm^2)	96.084

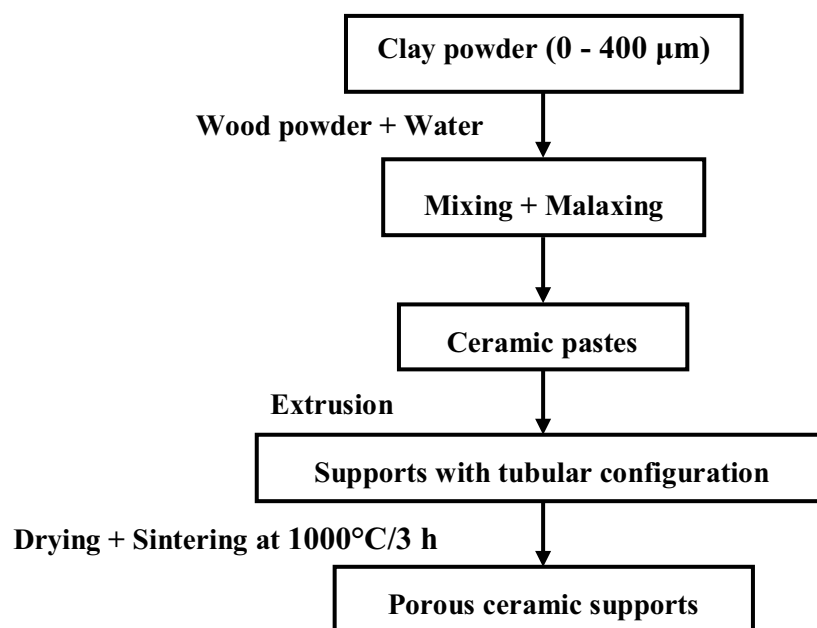


Fig. 1. Stages of the preparation of porous tubular ceramic supports through extrusion method.

membrane without defects. After drying at a room temperature, the microfiltration membranes are treated at 250°C for 2 h before being sintered at 900°C for 3 h. The heating rates for the two temperature intervals are respectively 1°C/min and 2°C/min. The optimum compositions for the supports and membranes' layers are mentioned in Table 3. The stepwise preparation method of ceramic microfiltration membranes' layers by the slip-casting technique is shown in Fig. 2. The mechanism of membranes' deposits formation on porous tubular supports is depicted in Fig. 3.

2.5. Cross-flow microfiltration pilot treatment

The DWW and the CR dye were treated by the cross-flow microfiltration pilot through the three reference microfiltration membranes: M10/25PVA, M10, and M12 (Fig. 4). The pilot was equipped with an electric pump with an adjustable flow, a pressure gauge, a safety valve, a membrane module, a pressure regulator, a filtered water collection (permeate) and a feed reservoir. The permeate was collected and characterized systematically every 15 min during filtration time of 1 h and 45 min. Filtration efficiency was evaluated by permeate flux, pH, electrical conductivity, COD, SPM, rate of turbidity removal and rate of discoloration. All cross-flow microfiltration tests are conducted at room temperature (25°C) with a 1 bar circulation pressure. Permeate flux (J , L/h m²) of membranes was determined using standard expression [Eq. (6)] [34]:

$$J(\text{L h}^{-1} \text{m}^{-2}) = \frac{V}{A \cdot t} \quad (6)$$

where V is the volume of permeate (L), A is the filtering surface (m²) and t is the filtration time (h).

3. Results and discussion

3.1. Characterization of the clay powder

3.1.1. Chemical analysis by X-ray fluorescence

The chemical analysis of our clay by XRF shows that the clay is rich in oxides of silicon (SiO₂), aluminum (Al₂O₃), and calcium (CaO) about 88 (wt.%), which explains the mechanical performance of this clay. On the other hand, we have very low percentages of alkaline and alkaline-earth oxides (Na₂O, K₂O, and MgO). The presence of iron oxide

(5.10 (wt.%)) explains the red coloration appearance of supports and membranes after heat treatment (Table 4).

3.1.2. Specific surface area and pore size distribution

Fig. 5 shows the adsorption-desorption isotherm of nitrogen at 77 K, carried out on a sample of our clay in the raw state. It shows that the isotherm obtained is type IV with a type H3 hysteresis loop, following the IUPAC (International Union of Pure and Applied Chemistry) classification characteristic of mesoporous solids [40]. The specific surface obtained by the BET method is 60 m²/g.

The PSD is based on the desorption or adsorption isotherm analysis. The principle of the PSD method is based on a discrete analysis of the isotherm desorption branch because it corresponds to a more thermodynamically stable equilibrium [41]. Fig. 6 gives the curve of this distribution for clay in the state gross. It shows that the diameters of the pores vary between 29 and 45 Å with a maximum distribution around 39 Å, indicating the presence of the mesopores. The raw clay's pore volume is measured at 0.08 cm³/g.

3.1.3. X-ray diffraction

The XRD is carried out on the raw clay powder and heat-treated at 1,000°C for 2 h. The results obtained are shown in Fig. 7. The diffractogram of the raw clay (Fig. 7a) shows, on the one hand, the presence of the mineral phases of silica in the form of quartz (Q), calcium carbonates (C), and feldspar (f), and on the other hand, we have kaolinite (K), illite (I), and smectite (S). The latter are the main phyllosilicate mineral phases present in the clay studied. Heat treatment of the clay at 1,000°C for 2 h (Fig. 7b) reveals the following results:

- The disappearance of reflections from the kaolinite (K) phase to provide meta-kaolinite ((Al₂O₃, 2SiO₂) (mk), which is an amorphous phase), this phenomenon which was observed by several authors [42–44] is subsequently confirmed by the infrared absorption spectroscopy and differential thermal and gravimetric analysis.
- A quartz transformation from an allotropic variety (α) to (β) [45].
- The total disappearance of calcium carbonate reflections (CaCO₃) and reflections specific to the illitic and feldsparic phase [46].
- The appearance of new mineral phases, namely mullite (3Al₂O₃, 2SiO₂) (M), and calcium aluminum silicate (CaO, Al₂O₃, 2SiO₂) (cas), and also the transformation of a part

Table 3

The optimum composition of raw materials used for the ceramic microfiltration membranes fabrication (support + membrane layer)

Ceramic microfiltration membrane	Composition of the support (% (w/w))	Composition of the membrane layer (% (w/w))
M10	85% (w/w) Clay, 15% (w/w) Wood powder, 33% (w/w) Water	10% (w/w) Clay, 90% (w/w) Water
M12	85% (w/w) Clay, 15% (w/w) Wood powder, 33% (w/w) Water	12% (w/w) Clay, 88% (w/w) Water
M10/25PVA	85% (w/w) Clay, 15% (w/w) Wood powder, 33% (w/w) Water	10% (w/w) Clay, 25% (w/w) Polyvinyl alcohol (12% (w/w) aqueous solution), 65% (w/w) Water

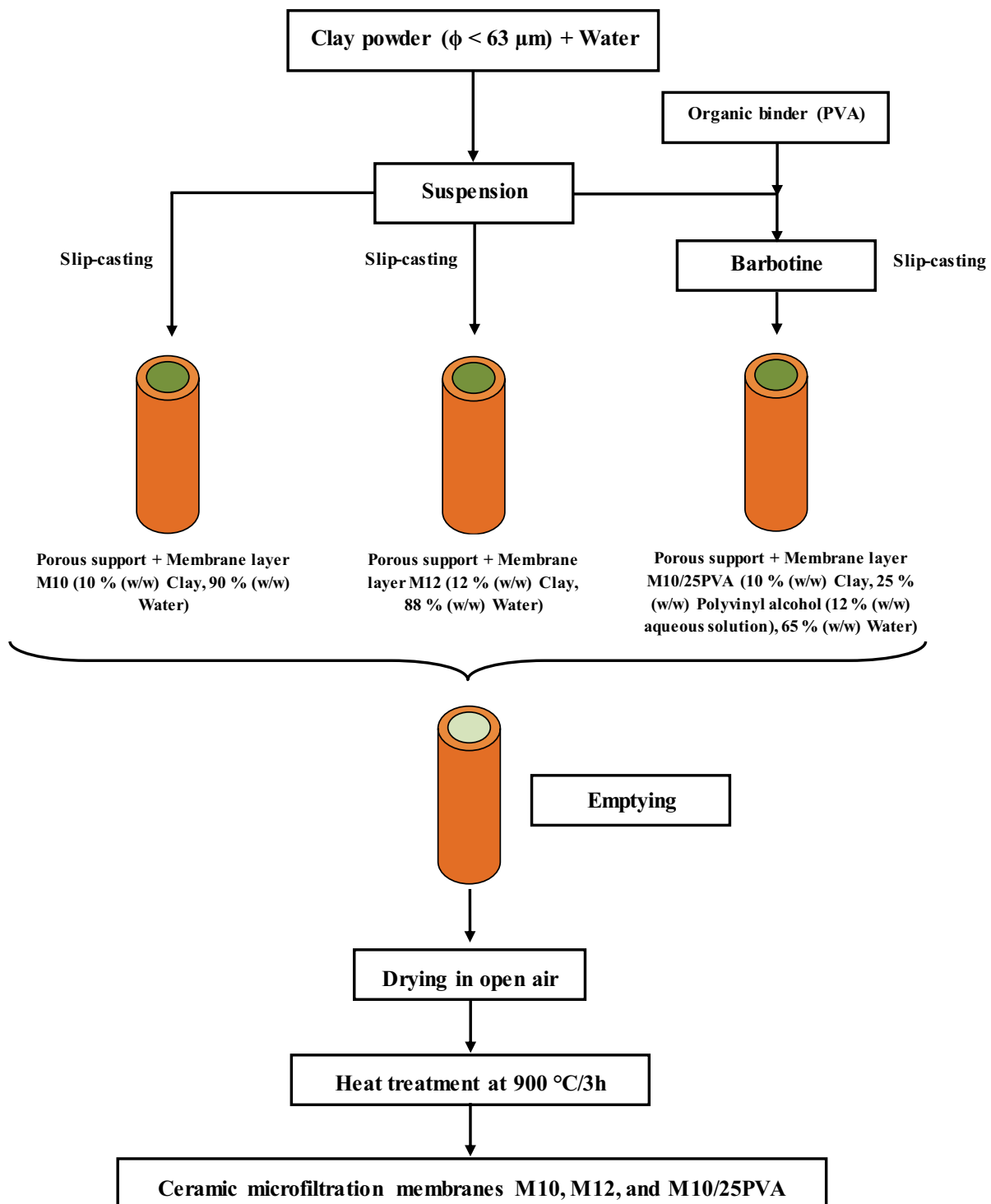


Fig. 2. Preparation of ceramic microfiltration membranes' layers by the slip-casting technique.

of beta quartz in beta cristobalite (cb) then in gamma tridymite (t) [47,48].

3.1.4. Infrared spectroscopy

The results obtained (Fig. 8a) show that the infrared spectra are very similar in the characteristic regions of clay

(3,750–3,300 cm^{-1}), (3,000–1,800 cm^{-1}), (1,450–1,400 cm^{-1}), (1,200–900 cm^{-1}), and (900–400 cm^{-1}) which corresponds to the valence vibrations and deformation of structural hydroxides: the organic fraction, the carbonates, the water of constitution, the groups (Si, Al, Fe)–O, and the appearance of new products during heat treatment. The characteristic bands of this clay have been attributed as follows:

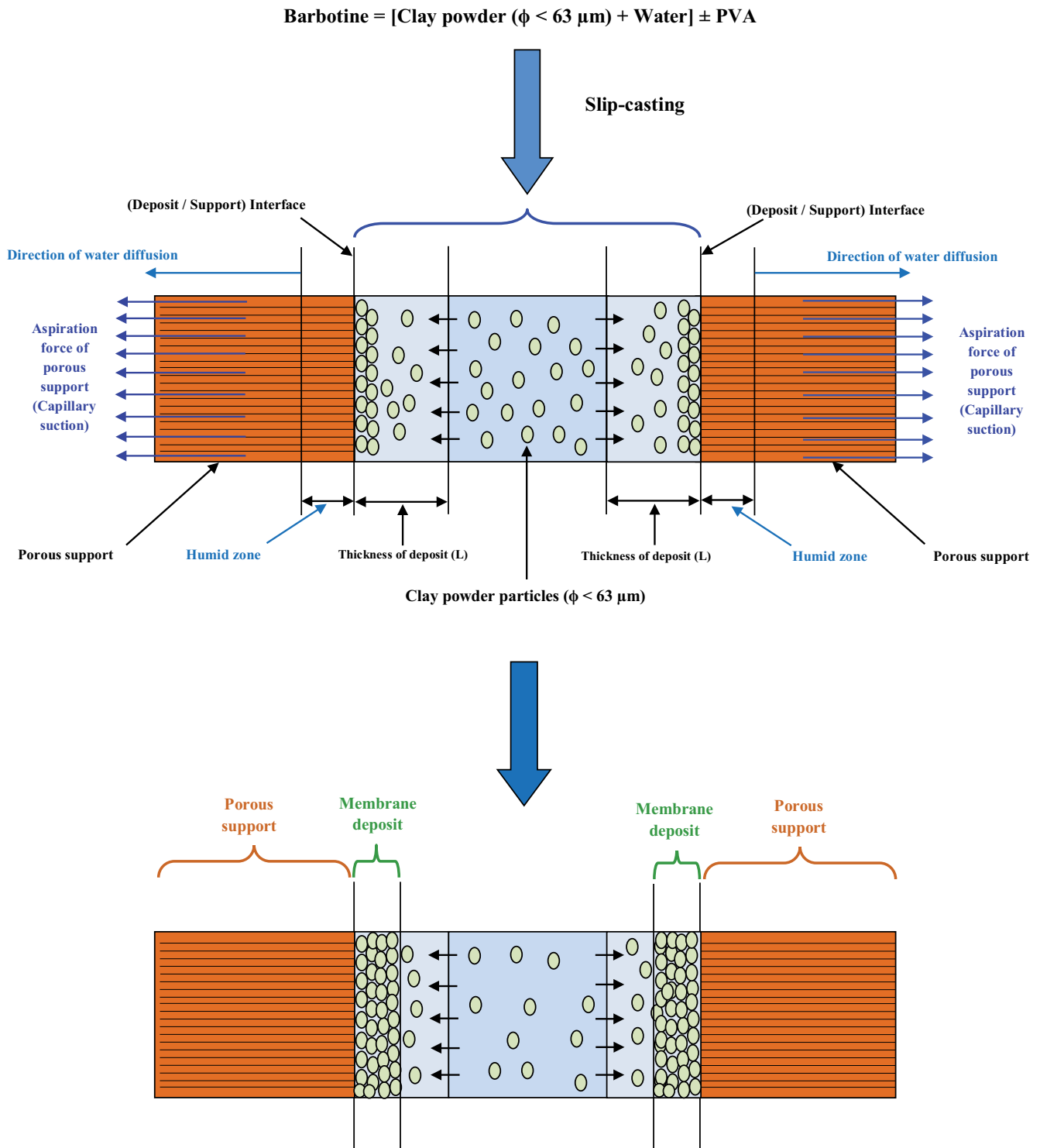


Fig. 3. Mechanism of membranes' deposits formation on porous tubular supports.

- In the interval $3,750\text{--}3,300 \text{ cm}^{-1}$: the first two bands $3,698 \text{ cm}^{-1}$ (a) and $3,620 \text{ cm}^{-1}$ (b) are attributable to the valence vibrations of the structural hydroxides of kaolinite $\nu(\text{OH})\text{-Al}$ [40–43]. The third band ($3,407 \text{ cm}^{-1}$ (c)) is attributed to the valence vibration of the group $\nu(\text{OH})$ of water absorbed by KBr or hygroscopic water [49,50].
- In the band $1,800 \text{ cm}^{-1}$ (d), we notice traces of organic matter attributed to the vibration of the C–H and/or C–O bond [51].
- The band at 1640 cm^{-1} (e) is due to the binding vibration of adsorbed water molecules $\delta(\text{OH})$ [52–54].
- The vibrations at $1,425 \text{ cm}^{-1}$ (f) and 872 cm^{-1} (i) are

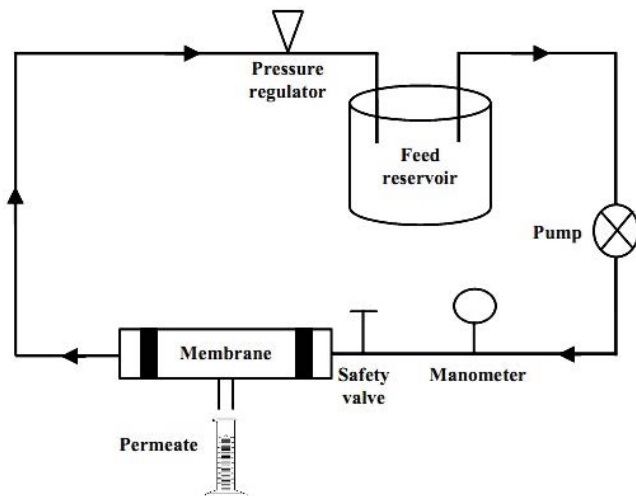


Fig. 4. Cross-flow microfiltration pilot.

Table 4
Chemical analysis of clay

Oxides	wt.%
SiO ₂	57.61
Al ₂ O ₃	16.97
CaO	13.20
Fe ₂ O ₃	5.10
MgO	2.60
MnO	0.11
Na ₂ O	0.67
K ₂ O	2.60
P ₂ O ₅	0.30
SO ₃	0.10
SrO	0.12
ZnO	0.01
Cr ₂ O ₃	0.02
TiO ₂	0.59

assigned to the vibrations of the carbonate group (CO₃²⁻) [53].

- The two bands 984 cm⁻¹ (g) and at 900 cm⁻¹ (h) are attributed to the deformation vibrations of the δ(OH)-Al [49,50,53].
- In the interval 900–400 cm⁻¹: we observed elongation vibrations Si–O–Si of the quartz bond at 798 cm⁻¹ (j) [52] and 778 cm⁻¹ (k) [53]. Besides, we have deformation vibrations of the bond δ(Si–O–Si) located at 693 cm⁻¹ (l), 450 cm⁻¹ (n) [49,50], and 413 cm⁻¹ (o). Furthermore, we noticed deformation vibrations of the δ(Si–O–Al) bond of kaolinite at 500 cm⁻¹ (m) [53].

In Fig. 8b, the disappearance of the majority of bands after treatment at 1,000°C for 2 h means that more than 80% of the bands disappeared, and the appearance of new bands but with very low intensity at 650 cm⁻¹ (cas) signified a characteristic vibration of a calcium aluminum silicate and at 560 cm⁻¹ (M) that implies a characteristic vibration of

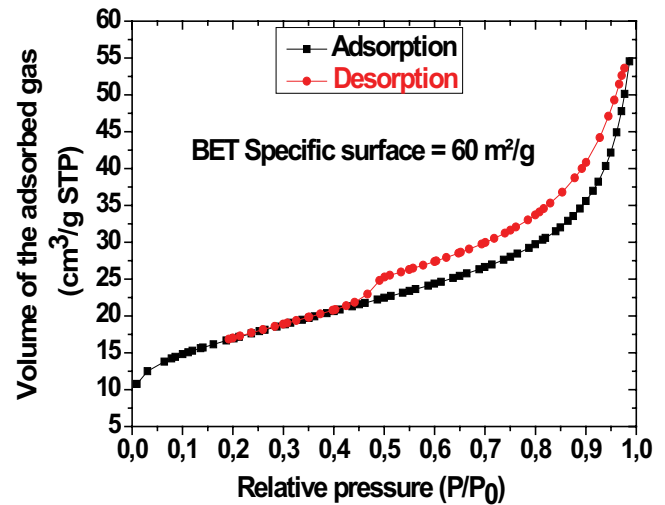


Fig. 5. Adsorption–desorption isotherm of nitrogen at 77 K of the powder clay in the raw state.

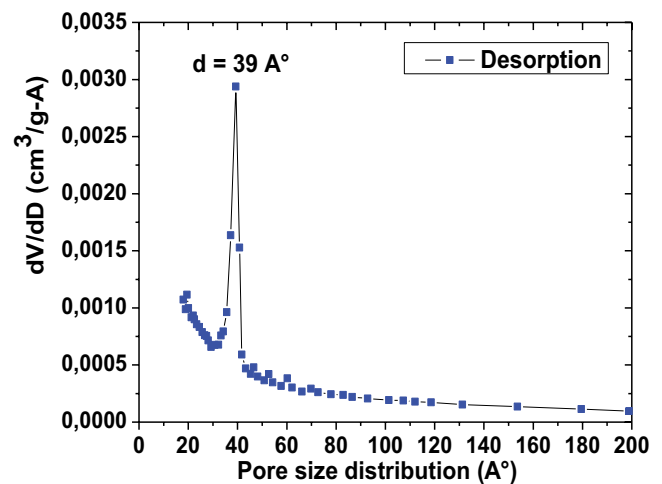


Fig. 6. Pore size distribution for the raw clay.

mullite. These results are confirmed by the above analysis of XRD (Fig. 7b).

3.1.5. Thermogravimetric analysis and differential thermal analysis

The TGA curve of the clay (Fig. 9) shows that during heating two main weight losses occur in two distinct stages with a third continuous and slight loss. The first loss (2.44%) which begins around 31°C and ends around 250°C corresponds to that of the water absorbed, and the second (12.14%) begins around 300°C and ends around 750°C is mainly due to the dehydroxylation of kaolinite. On the DTA curve, we observe five endothermic peaks:

- The peak around 73°C corresponds to the departure of absorbed water or moisture.
- The peak around 140°C is due to the departure of zeolitic water (inter-leaf water) [55,56]. The crystal structure of the clay is not destroyed by removing these two types of water.

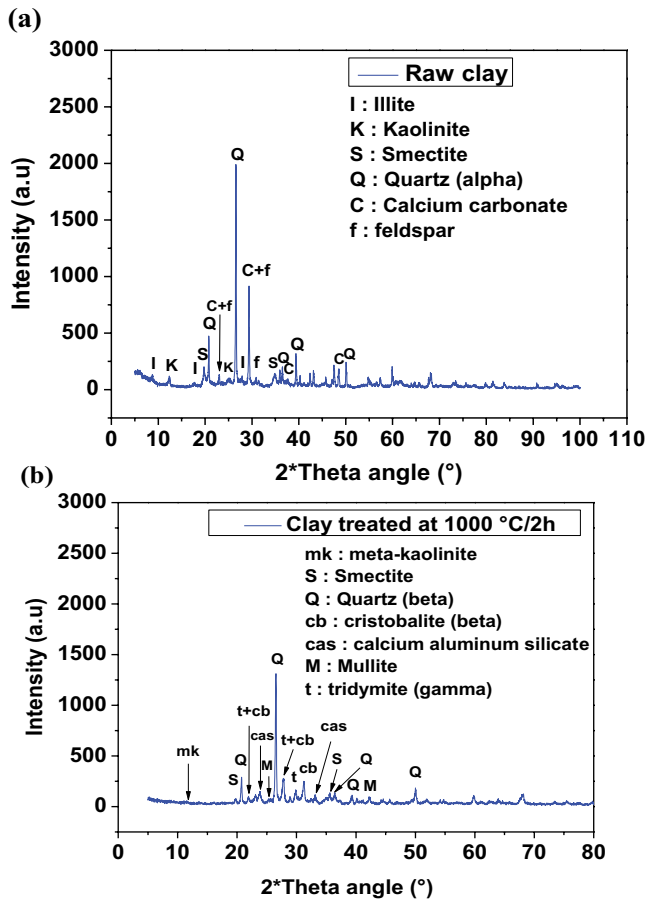


Fig. 7. X-ray diffractograms of raw clay (a) and treated clay (b) at 1,000°C/2 h.

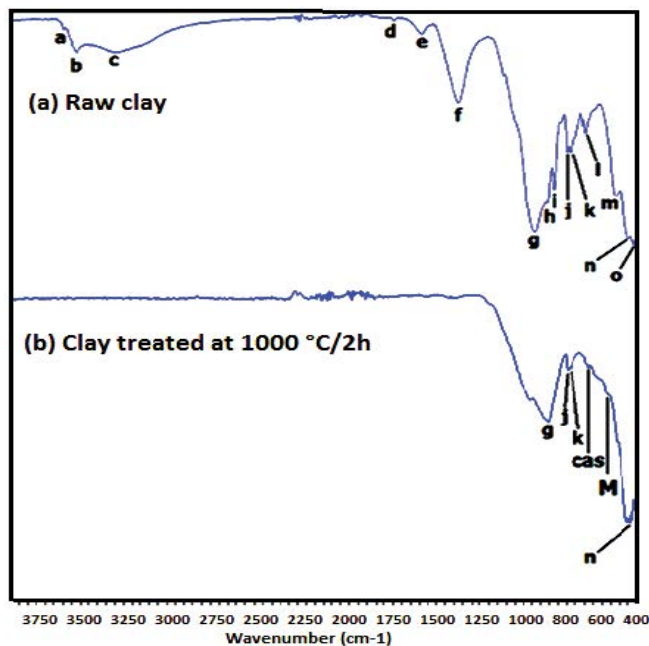


Fig. 8. FTIR spectra of raw clay (a) and treated clay (b) at 1,000°C for 2 h.

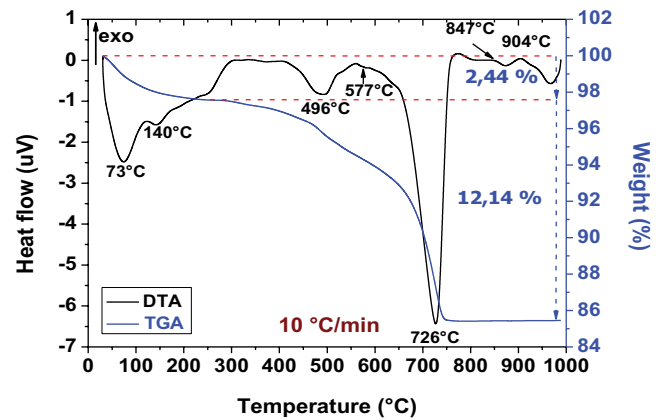
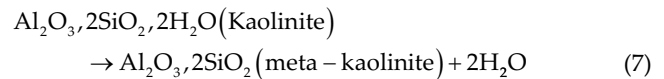
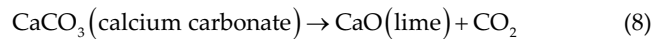


Fig. 9. TGA and DTA curves for clay powder.

- The peak around 496°C corresponds to the dehydroxylation of kaolinite ($\text{Al}_2\text{O}_3, 2\text{SiO}_2, 2\text{H}_2\text{O}$) to meta-kaolinite ($\text{Al}_2\text{O}_3, 2\text{SiO}_2$, amorphous phase) [57]. That is, as water is removed from a structure, the crystalline structure of the mineral is destroyed. The overall dehydroxylation reaction can be schematized as follows [58]:

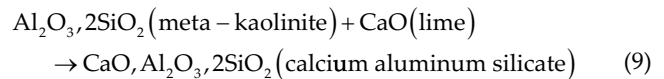


- The peak around 577°C is very weak; it illustrates the transformation of quartz from the allotropic variety (α) to (β).
- The peak around 726°C is due to the decomposition of calcium carbonate according to the following reaction:

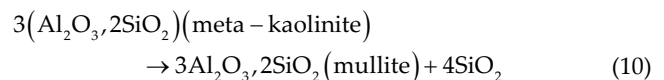


We observe on the same curve, two exothermic peaks around 847°C and 904°C and are due, respectively:

- The formation of a calcium aluminum silicate ($\text{CaO}, \text{Al}_2\text{O}_3, 2\text{SiO}_2$) by combining lime (CaO) and meta-kaolinite ($\text{Al}_2\text{O}_3, 2\text{SiO}_2$) according to the following reaction:



The crystallization of mullite ($3\text{Al}_2\text{O}_3, 2\text{SiO}_2$) from amorphous oxides or meta-kaolinite ($\text{Al}_2\text{O}_3, 2\text{SiO}_2$) according to the following reaction [59]:



3.2. Characterization of ceramic microfiltration membranes

3.2.1. Morphology and EDX analysis

The micrographs obtained by the SEM show a good arrangement of the spherical particles of the clay

powder under the effect of the final sintering temperature (900°C/3 h). Grain boundaries are observed at the surface joining the microfiltration layers (M10/25PVA, M10, and M12) and the porous supports; this ensures good adhesion between the microfiltration layer and the support. In addition to a statistically well-distributed porosity over the entire microfiltration membranes' surfaces (Fig. 10a–c), we note that the surfaces are homogeneous and without defects because there are no agglomeration and cracks.

The EDX analysis of the microfiltration membranes' surfaces shows that the intensity of the peaks of silicon (Si), aluminum (Al), and calcium (Ca) characteristic of the oxides SiO_2 , Al_2O_3 , and CaO , respectively appear very high in the M10/25PVA, M10, and M12 microfiltration layers' surface (Fig. 11). These observations are perfectly confirmed by the chemical analysis of the raw clay (Table 4). Additionally, it is important to note from these EDX spectra that the

elementary chemical composition of the microfiltration membranes' surfaces is predominated by the elements Si, Al, Ca, and Fe.

3.2.2. Pore diameter and permeation flux

The average pore diameters of membranes are determined as 1.31, 1.21, and 1.76 μm for M12, M10, and M10/25PVA, respectively that correspond to microfiltration range ceramic membrane (Table 5). The initial mass composition of each membrane layer is justified by the difference in pore diameter from one membrane to another. The average pore diameter of the M10 membrane increases from 1.21 to 1.76 μm for the M10/25PVA membrane, indicating the influence of the incorporation of the PVA. Comparably, the permeation flux increases from 881 to 908 $\text{L/h m}^2 \text{ bar}$ for the membranes M10 and M10/25PVA, respectively (Fig. 12).

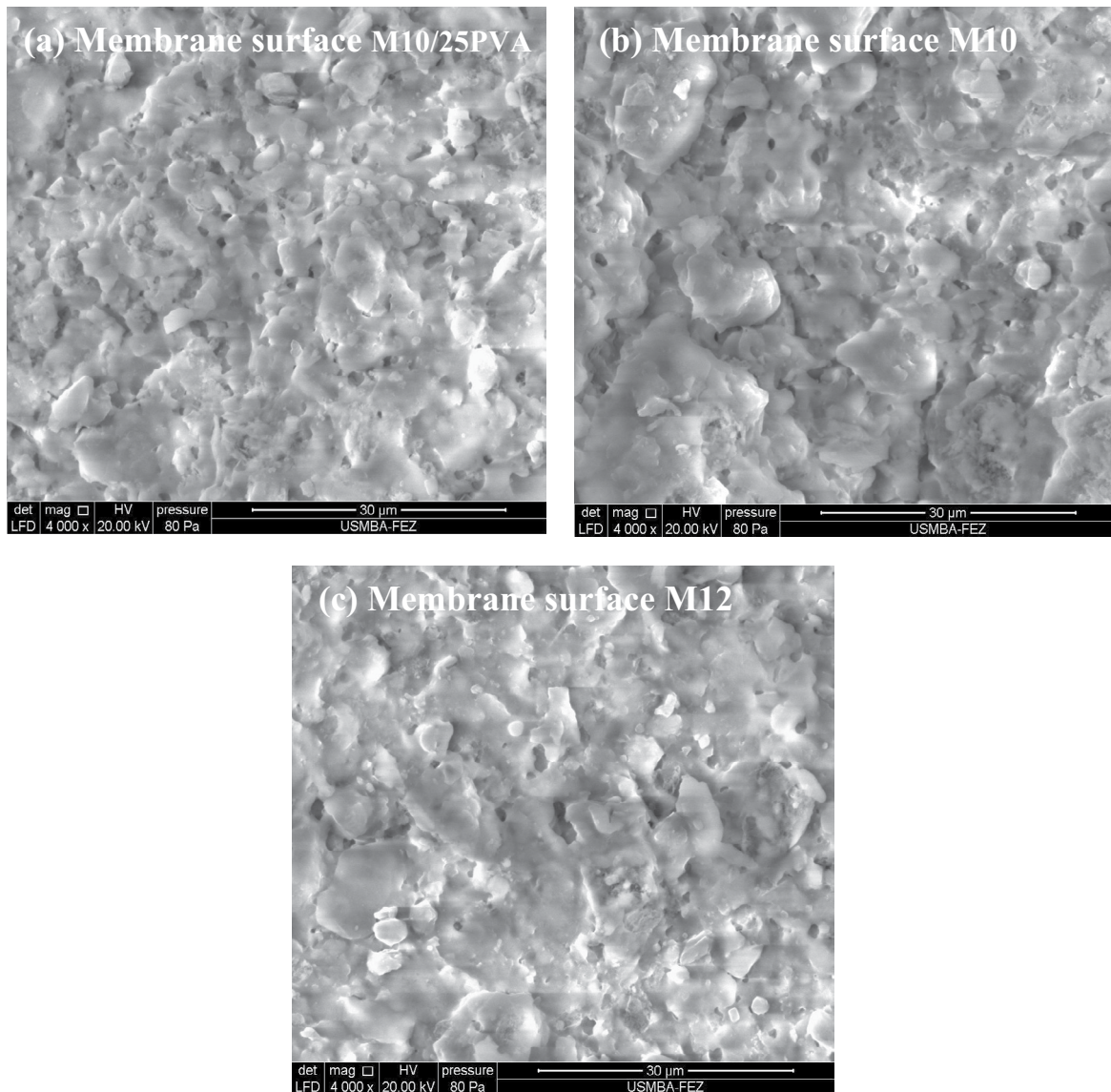


Fig. 10. SEM of ceramic microfiltration membranes' surfaces sintered at 900°C/3 h: M10/25PVA (a), M10 (b), and M12 (c).

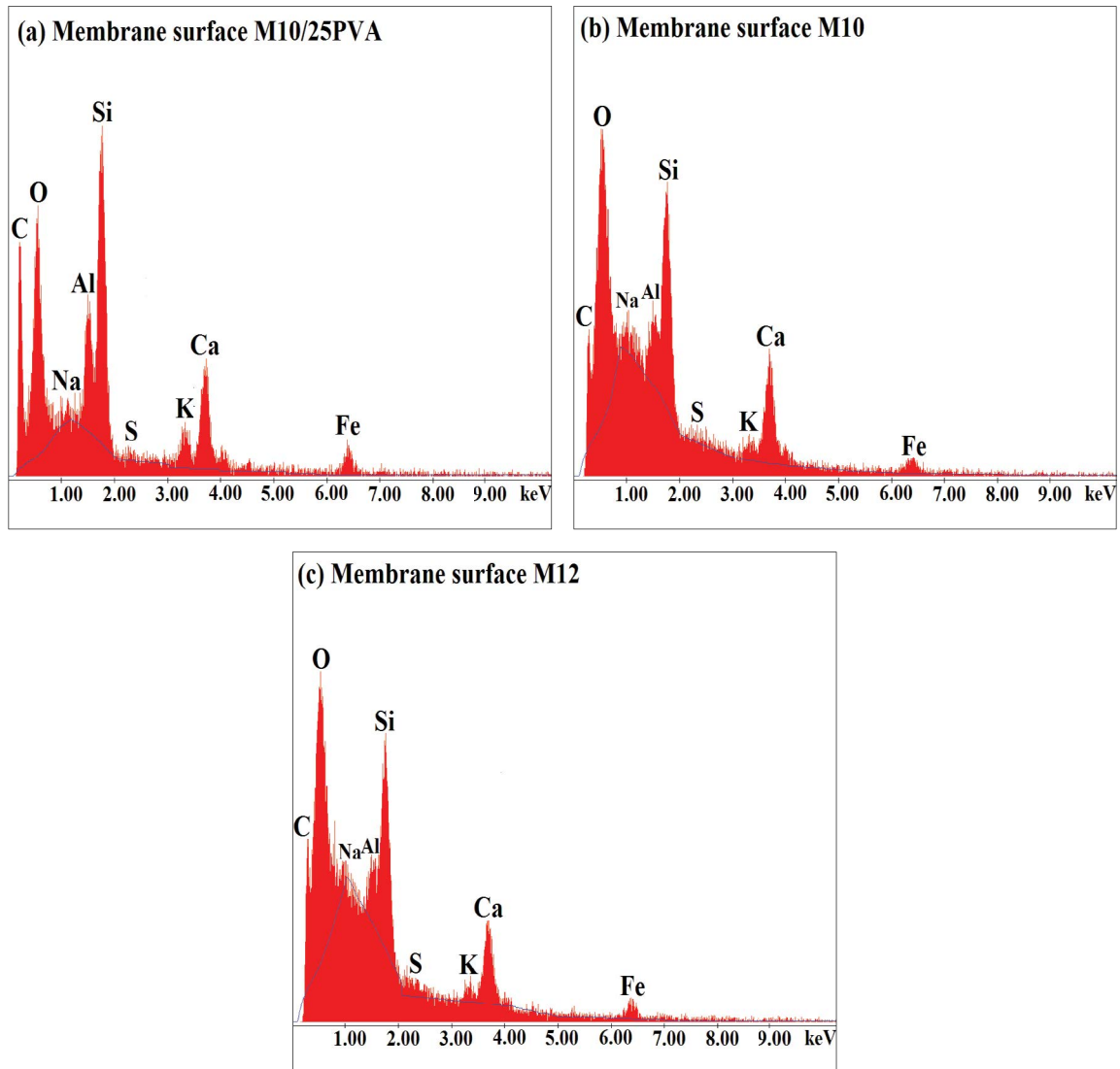


Fig. 11. EDX analysis of membranes' surfaces M10/25PVA (a), M10 (b), and M12 (c).

Table 5
Characteristics of the ceramic microfiltration membranes

Ceramic membrane	Permeation flux (L/h m ² bar) [39]	Average pore diameter (μm)	Filtration area (cm ²)
M10/25PVA	908	1.76	≈96.084
M10	881	1.21	≈96.084
M12	696	1.31	≈96.084

3.2.3. Chemical resistance

Chemical resistance of the sintered membranes was checked in terms of weight loss in contact with acids or bases. A small part of the ceramic membranes was kept in acidic conditions in contact with HNO₃ (pH = 0.5) and alkali NaOH solution (pH = 13.6) individually for 24 consecutive hours at 25°C with stirring; and the net weight loss was calculated after drying. The stability in terms of all membranes weight loss for the acid contact HNO₃ (varies

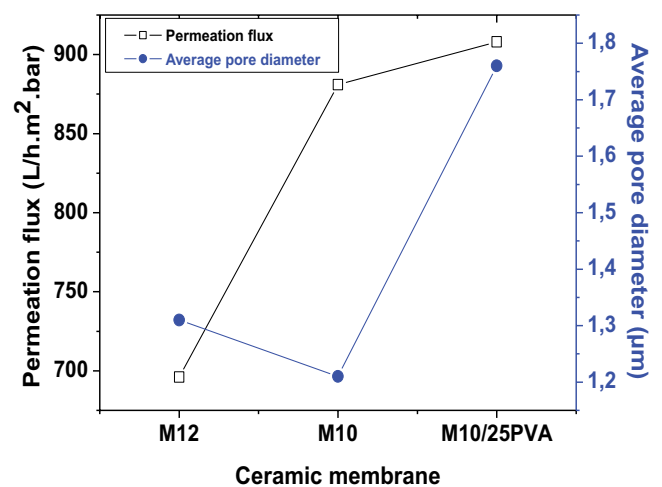


Fig. 12. Permeability flux and average pore diameter at different membranes fabrication.

between 0.11% and 0.16%). And for the basic contact NaOH (varies between 0.21% and 0.42%). Stability towards acidic conditions is found to be higher as compared to the basic condition. This result is in good agreement with the trends found in the literature [60].

3.3. Treatment of DWW from the city of Meknes

The DWW samples were collected from a river in Meknes, more specifically near the ASSALM swimming pool. DWW samples are stored in 30 L polyethylene tanks at 4°C before being sent to the laboratory for analysis. The characteristics of DWW used in this study are summarized in Table 6. The DWW is characterized by alkaline pH and low electrical conductivity, which indicates low salinity. The turbidity of DWW is comparatively high (201 NTU), attributed to the presence of suspended particles from various sources (e.g., bacteria, micro-organisms, colloid aggregates, etc.). High SPM content (400 mg/L). The COD value of 8.81 mg/L in the DWW sample is related to the presence of organic and inorganic compounds that may be caused by fouling and biological fouling membranes.

3.3.1. Evolution of the permeation flux as a function of time

The DWW was filtered on the three ceramic microfiltration membranes (M10/25PVA, M10, and M12) using the pilot described in Fig. 4, and Fig. 13 illustrates the evolution of DWW permeate flux during filtration time.

The permeate flux for the three membranes decreases during the first minutes before stabilizing after 60 min of filtration at values of 110, 63, and 52 L/h m² for the membranes M10/25PVA, M10, and M12, respectively. The decrease is caused by the adsorption and deposition of SPM and micro-organisms partially clogging the pores. Following that, the accumulation of the particles with a diameter approximately equal to the diameter of the pores forms a concentration polarization layer [61]. The permeation flux can also be classified in the following order: Flux_(M10/25PVA) > Flux_(M10) > Flux_(M12). The difference in thicknesses and the morphological structure of microfiltration membrane's layers explains the above order. Therefore, the filtration flux decreases as the filter layer thickness increases.

3.3.2. Evolution of pH and electrical conductivity over time

The obtained results (Fig. 14) show that the pH values have remained quasi constant during all microfiltration studies. After 45 min of filtration, the electrical conductivity

Table 6
Physicochemical characteristics of DWW

Physicochemical parameters	Values
T (°C)	26.5
pH	8.08
Electrical conductivity (µs/cm)	893
COD (mg/L)	8.81
SPM (mg/L)	400
Turbidity (NTU)	201

of the membranes M10/25PVA (Fig. 14a), M10 (Fig. 14b), and M12 (Fig. 14c) decreased from 893 to 811, 810, and 801 µs/cm, respectively. After this reduction, there is a near stabilization. Due to the low load of dissolved salts in the DWW studied, the adsorption of dissolved salts on the filtering surface of the ceramic membranes may explain the decrease in conductivity. The conductivity is not rejected by M10/25PVA, M10, or M12 membranes, as expected, because the average pores diameter are larger to retain soluble salts.

3.3.3. Effect of membranes on COD

After 15 min of filtration, the three ceramic microfiltration membranes display a decrease in COD (Fig. 15). The values range from 8.81 to 7.13, 7.21, and 7.31 mg/L for membranes M10/25PVA (Fig. 15a), M10 (Fig. 15b), and M12 (Fig. 15c), respectively. Adsorption and biochemical degradation of dissolved organic material during filtration may explain the reduction in COD.

3.3.4. Effect of membranes on turbidity

The three ceramic microfiltration membranes eliminated suspending and colloidal matter from the DWW, as shown in Fig. 16. The turbidity removal efficiency of the three ceramic membranes M10/25PVA (Fig. 16a), M10 (Fig. 16b), and M12 (Fig. 16c) will exceed 99%, due to the creation of a cake layer on the inner membrane surface. This indicates the effectiveness of our manufactured ceramic membranes.

Table 7 summarizes the physicochemical characteristics of the DWW and filtered after one hour of filtration by the three ceramic microfiltration membranes M10/25PVA, M10, and M12. The results show that the turbidity caused by particulate suspending matter has been fully eliminated. COD has decreased significantly. The pH of the permeate is remained constant over the filtration test, although there was a slight decrease in electrical conductivity.

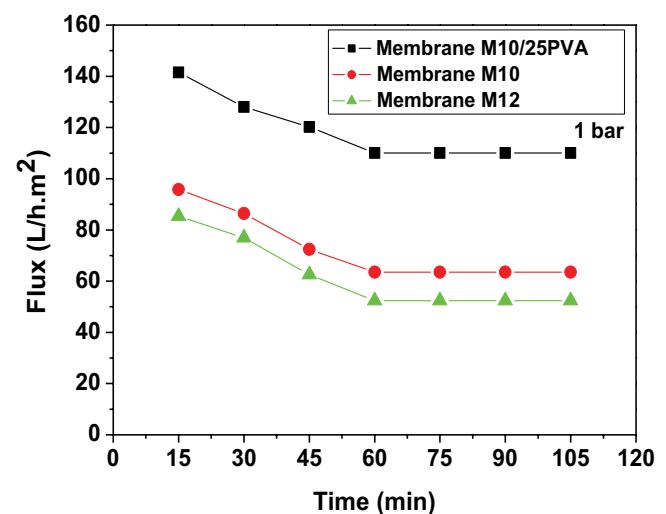


Fig. 13. Variation in the permeate flux of the DWW as a function of time for the three ceramic membranes M10/25PVA, M10, and M12 (Experimental conditions: pressure = 1 bar, temperature = 25°C).

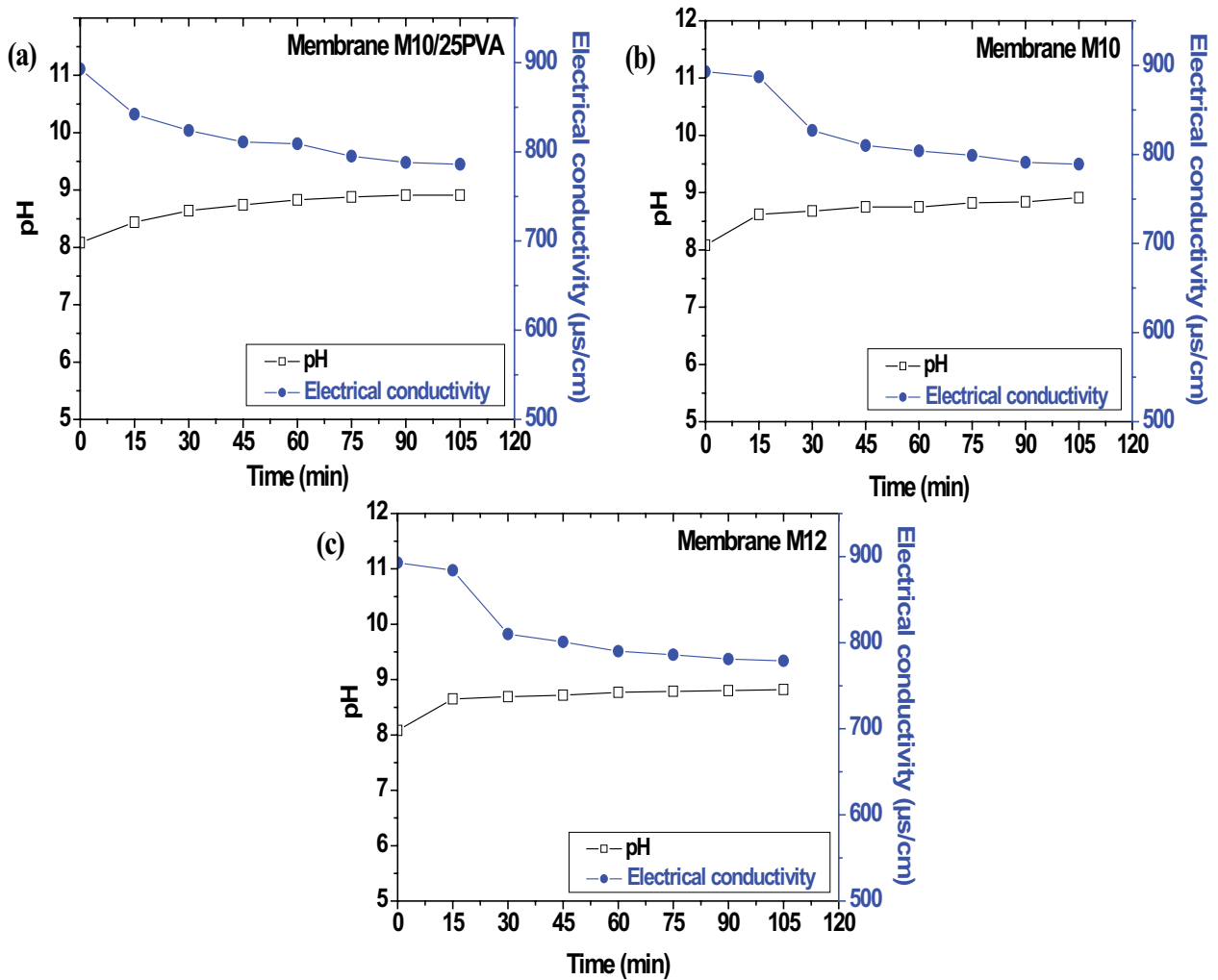


Fig. 14. The evolution of the pH and electrical conductivity of the DWW permeates as a function of time for the three ceramic membranes M10/25PVA (a), M10 (b), and M12 (c), (Experimental conditions: pressure = 1 bar, temperature = 25°C).

3.4. Treatment of CR dye by cross-flow microfiltration

3.4.1. Evolution of the permeation flux as a function of time

In the first step, we prepared a colored solution of CR (0.2 g/L), and in a second step, we investigated the treatment of this dye by the three ceramic membranes produced (M10/25PVA, M10 and M12). Fig. 17 illustrates, as a function of time, the variation in the permeate flux of the CR.

The permeate flux of the three ceramic membranes stabilizes after 60 min of filtration at 150, 100, and 80 L/h m², respectively for the M10/25PVA, M10, and M12 membranes. The decrease in the permeate flux is due to adsorption and partial blockage of the pores by macro-molecules of the studied dye and subsequently, the phenomenon of concentration polarization is observed [61]. The nature and thickness of the filter layer account for the difference in permeation flux obtained with ceramic membranes, as well as the characteristics of the colored solution, such as viscosity and molecular size (the chemical structure and the molecular weight).

3.4.2. Discoloration rate of CR as a function of time

The visible Ultra-Violet spectrum of CR solution shows two characteristic bands λ_1 and λ_2 located at 530 and 566 nm, respectively (Fig. 18).

According to the findings obtained, the CR discoloration rate of all membranes varies between 91% and 99% for two characteristic bands λ_1 and λ_2 . Therefore, the anionic dye and the membranes' surfaces likely have repulsive interactions, which could contribute to relatively high CR rejection. According to the dye rejection, it can be inferred that the prepared microfiltration membranes shows competitive performances in terms of selectivity.

We compared the elimination rate (%) of our ceramic microfiltration membranes with that of other membranes in this study. We conclude that the order of elimination rate obtained for DWW and CR namely turbidity elimination rate (R_t) and discoloration rate (R_d) is similar compared to the others. It can be observed that all the membranes performed satisfactorily in terms of removing the turbidity and discolor colored rejections. To do a comparison

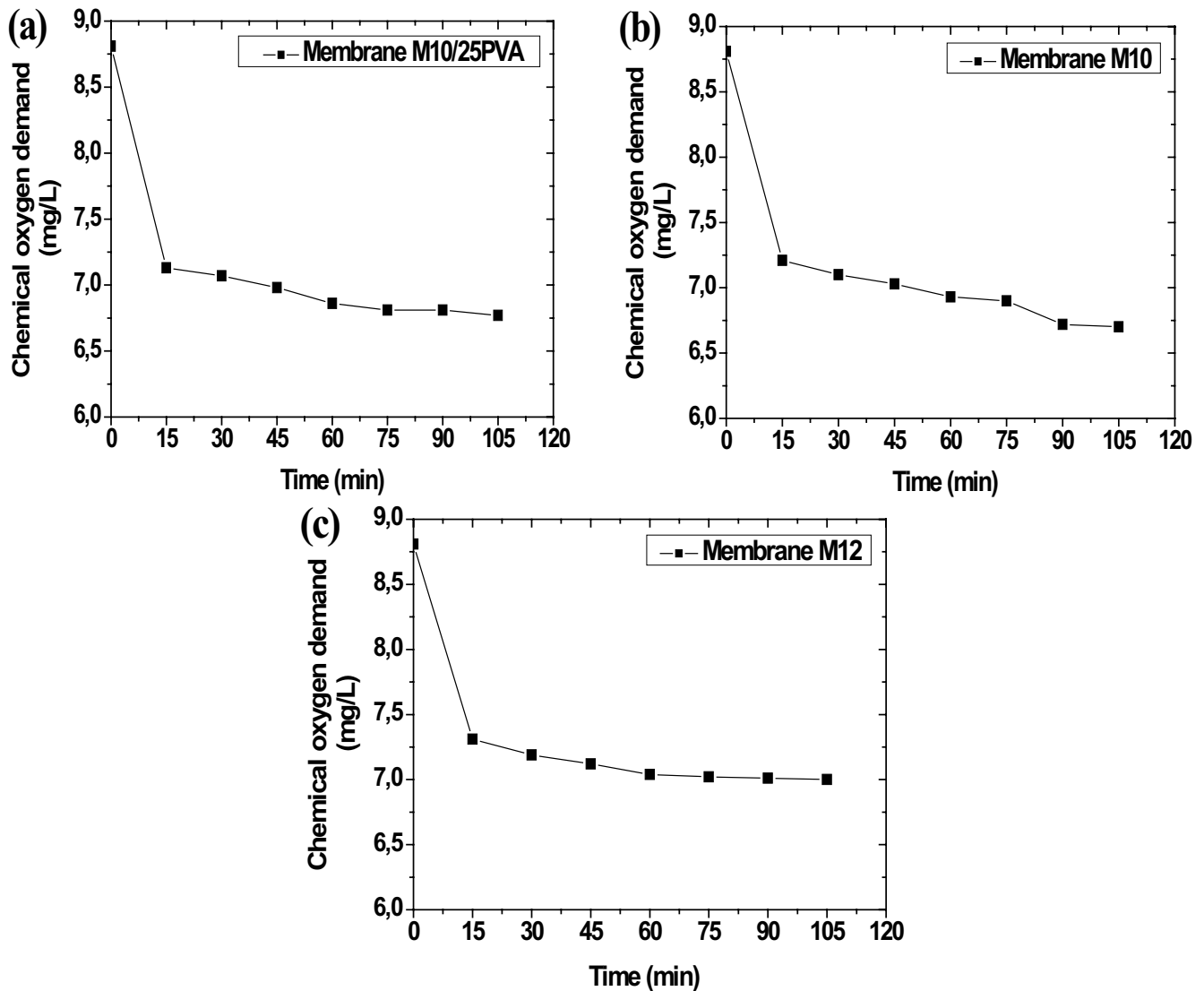


Fig. 15. Evolution of COD as a function of time for the three ceramic membranes M10/25PVA (a), M10 (b), and M12 (c), (Experimental conditions: pressure = 1 bar, temperature = 25°C).

Table 7

Characterization of the DWW and various permeates recovered after 1 h of filtration (Experimental conditions: pressure = 1 bar, temperature = 25°C)

Physicochemical characteristics	DWW	M10/25PVA Permeate	M10 Permeate	M12 Permeate
pH	8.08	8.83	8.75	8.77
Electrical conductivity ($\mu\text{s}/\text{cm}$)	893	809	804	790
COD (mg/L)	8.81	6.86	6.93	7.04
SPM (mg/L)	400	0	0	0
Turbidity (NTU)	201	0.99	1.12	0.83
R_e (%)	–	99	99	99

between various microfiltration membranes fabricated and to highlight their effectiveness, the results of the three clayey ceramic membranes have been summarized and compared to those used in previous work in Table 8.

3.5. Cost analysis

The industrially competitive aspect of membrane technology lies in its cost. Generally, the high-cost ceramic

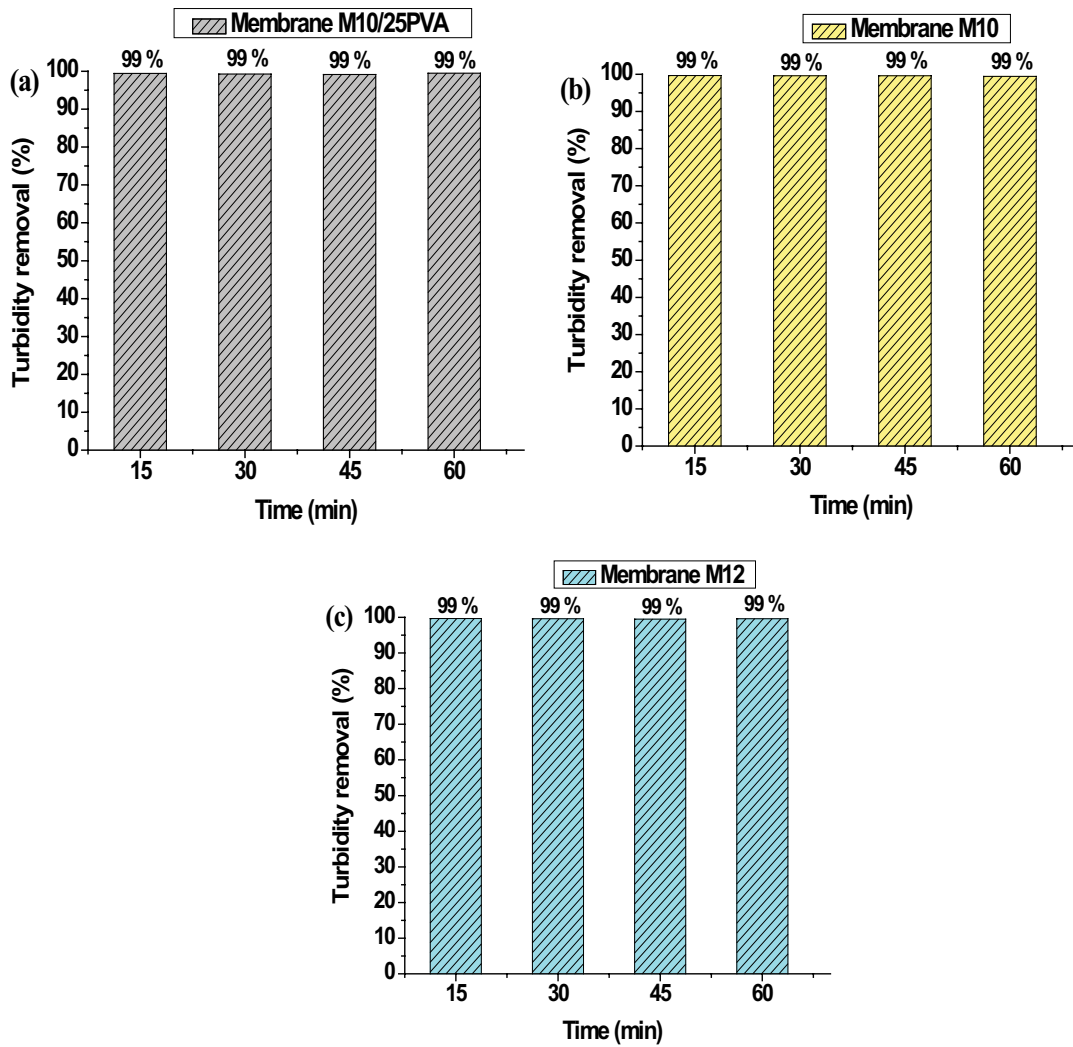


Fig. 16. Evolution of the turbidity removal efficiency of the permeates of the DWW as a function of time for the three ceramic membranes M10/25PVA (a), M10 (b), and M12 (c), (Experimental conditions: pressure = 1 bar, temperature = 25°C).

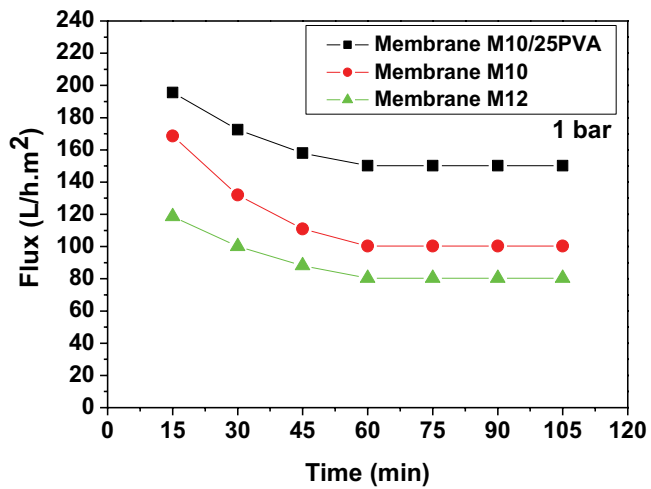


Fig. 17. Variation of the permeate flux of CR permeates as a function of time for the three ceramic membranes M10/25PVA, M10, and M12, (Experimental conditions: initial concentration of CR = 0.2 g/L, pressure = 1 bar, temperature = 25°C).

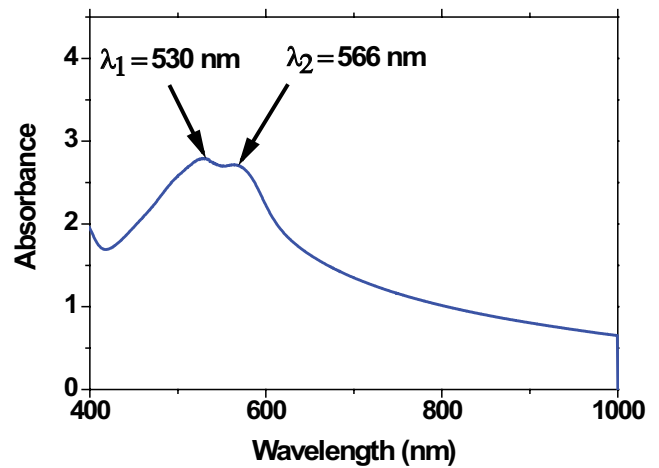


Fig. 18. Visible UV spectrum of CR.

Table 8
Comparative performance of M10/25PVA, M10, and M12 ceramic microfiltration membranes with other reported membranes

Membrane material	Membrane Configuration	Pollutant	Feed (Concentration/Turbidity)	Applied pressure (bar)	Elimination rate (%)	Reference
Nano-clay	Flat disk	Methylene blue (Cationic dye)	35.76 mg/L	1.5	90.23	[33]
		Crystal violet (Cationic dye)	54 mg/L	1	95.55	
		Methyl orange (Anionic dye)	–	–	10	
Kaolinitic clay	Tubular	Oily wastewater	921 mg/L	2	97.31	[35]
Cameroonian clay	Flat disk	Aqueous suspensions of clay powder	(1–2) g/L	5.5	97	[62]
		Tannery beam-house effluent	760 NTU		99.80	
Moroccan clay and phosphate	Flat disk	Raw seawater	120 NTU	0.14	99.62	[63]
		Synthetic solution of aluminum chloride	725 NTU		99.86	
Tunisian clay	Tubular	Seawater desalination	–	–	99	[64]
Kaolin-fly ash	Flat disk	Oily wastewater	300 mg/L	–	96.7–99.5	[65]
Moroccan pozzolan-clay	Tubular	Seawater	6.29 NTU	1	99.25	[66]
Kaolin-fly ash-dolomite	Flat disk	Oil-water	(100–200) mg/L	1	97.4–98.8	[67]
Polyethersulfone modified with polyethylenimine and graphene oxide	Flat disk	Blue corazol	≈40 mg/L	3	97.8	[68]
Membrane M10/25PVA (Moroccan clay)					99	
Membrane M10 (Moroccan clay)	Tubular	DWW	201 NTU	1	99	In this study
Membrane M12 (Moroccan clay)					99	
Membrane M10/25PVA (Moroccan clay)					97–99	
Membrane M10 (Moroccan clay)	Tubular	CR (Anionic dye)	0.2 g/L	1	97–99	In this study
Membrane M12 (Moroccan clay)					91–99	

membrane is compensated by its higher permeability and longer lifetime, which reduces the operating and maintenance cost. Several studies show that the conventional polymeric membranes available for industrial-scale operation cost around 50–200 \$/m² [69]. However, often inorganic membranes are quoted to be at least 10 times expensive than polymeric membranes and their cost is projected to be around 500–1,000 \$/m² [70]. The cost of three fabricated membranes was estimated based on the retail cost of the raw materials, and it was also compared with other studies. Table 9 shows the results obtained after a conceptual cost analysis made ceramic membranes that were the raw materials.

The cost analysis mentioned in the above table shows that natural clay is very preferred membrane materials over other materials due to its low raw materials cost. In our case, the estimated ceramic membranes cost varied between 21 and 23 \$/m². This is competitive to the cost of the commercially available membranes. As a result, when compared to membranes made from other raw materials, it can be inferred that the fabricated membranes are extremely cost-effective (Table 10).

4. Conclusion

In this work, a series of low-cost ceramic microfiltration membranes have been successfully prepared using

Table 9
Cost analysis of the fabricated ceramic membranes

		Unit price (\$/kg)	Amount of raw materials required for the fabrication of one ceramic membrane (g)		
			Membrane M10/25PVA	Membrane M10	Membrane M12
Raw materials of the membrane layer	Raw clay	0.1	10	10	12
	PVA (Organic binder)	0.8	25	0	0
	Distilled water	0.25	65	90	88
	Raw materials cost per membrane layer (\$)	–	0.037	0.024	0.023
	Raw materials cost per unit area of the membrane layer (\$/m ²)	–	3.85	2.50	2.39
Raw materials of the membrane support	Raw clay	0.1		850	
	Wood powder (Porosity agent)	0.02		150	
	Distilled water	0.25		330	
	Raw materials cost per membrane support (\$)	–		0.17	
	Raw materials cost per unit area of the membrane support (\$/m ²)	–		17.71	
Cost of energy-consuming during heat treatment (\$)	–		1.5		
Estimated total cost of the fabricated ceramic microfiltration membrane (Membrane layer + Membrane support) (\$/m ²)	–	23.06	21.71	21.60	

different compositions of raw materials by slip-casting technique. For all prepared membranes, the optimum sintering temperature is 900°C/3 h. As expected, the filtration properties and microstructure of the membranes are significantly affected by the sintering temperature. The prepared membranes have excellent permeation flux, pore diameter, and chemical resistance, and make them ideal for microfiltration applications. The permeation fluxes for the M10/25PVA, M10, and M12 membranes were found to be 908, 881, and 696 L/h m² bar, respectively. The weight losses of the membranes in acid and alkali solutions are found to be 0.11%–0.16% and 0.21%–0.42%, respectively. This indicates that these ceramic membranes are more stable in both acidic and basic environments. The average pore sizes of the membranes calculated from the SEM images data are found to be 1.76, 1.21, and 1.31 μm for membranes M10/25PVA, M10 and M12, respectively.

The cross-flow microfiltration treatments of DWW from Meknes-Morocco, and a synthetic colored solution of CR dye were investigated using the fabricated membranes. The turbidity removal efficiency reaches 99%. The complete discoloration of CR is found to be 91%–99% for $\lambda_1 = 530$ nm and $\lambda_2 = 566$ nm. In terms of cost analysis, the results show that natural clay is much cheaper than the cost of the membranes which is estimated to be around 21–23 \$/m² due to the low raw material cost. These results suggest as our manufactured ceramic membranes may be used to remove turbidity from wastewater and to discolor colored solutions.

Authors Contributions

S. Iaich: Writing – original draft, review and editing, Y. Miyah: Review and editing, F. El Azhar: Review and

editing, S. Lagdali: Writing – original draft, M. El Habacha: Writing – original draft. All authors have read and agreed to the published version of the manuscript.

Funding

This research received no external funding.

Acknowledgments

The authors would like to appreciate the technical support of the European Institute of Membranes in Montpellier – France, for the measurement of the BET-PSD analyzes. The Regional University Interface Center at the Higher School of Technology of Fez – Morocco, for FTIR and SEM analyzes. The Research Center of the Faculty of Sciences of Meknes – Moulay Ismail University – Morocco, for the XRD and UV analyzes.

Declaration of interests

The authors declare that they have no known competing financial interests or personal relationships that could have appeared to influence the work reported in this paper.

Symbols and Abbreviations

XRF	–	X-ray fluorescence
BET	–	Brunauer, Emmett, and Teller
PSD	–	Pore size distribution
XRD	–	X-ray diffraction
FTIR	–	Fourier transform infrared
DTA	–	Differential thermal analysis
TGA	–	Thermo-gravimetric analysis

Table 10
Comparison of the manufacturing cost of ceramic microfiltration membranes

Raw materials for the manufacturing of ceramic microfiltration membrane (% (w/w))	Estimated total cost of the fabricated ceramic microfiltration membrane (\$/m ²)	Reference
Membrane SP1 (30% (w/w) Quartz, 20% (w/w) CaCO ₃ , 50% (w/w) Fly ash)	15	
Membrane SP2 (30% (w/w) Quartz, 20% (w/w) CaCO ₃ , 40% (w/w) Fly ash, 10% (w/w) TiO ₂)	25	
Membrane SP3 (30% (w/w) Quartz, 20% (w/w) CaCO ₃ , 30% (w/w) Fly ash, 20% (w/w) TiO ₂)	33	[20]
Membrane SP4 (30% (w/w) Quartz, 20% (w/w) CaCO ₃ , 20% (w/w) Fly ash, 30% (w/w) TiO ₂)	40	
Membrane M1 (50% (w/w) Kaolin, 25% (w/w) Quartz, 25% (w/w) Calcium carbonate)	54.53	
Membrane M2 (50% (w/w) Kaolin, 25% (w/w) Quartz, 22% (w/w) Calcium carbonate, 3% (w/w) Titanium dioxide)	55.53	[71]
Membrane M3 (50% (w/w) Kaolin, 25% (w/w) Quartz, 15% (w/w) Calcium carbonate, 10% (w/w) Titanium dioxide)	57.53	
MF membrane (40% (w/w) Kaolin, 15% (w/w) Quartz, 25% (w/w) Calcium carbonate, 10% (w/w) Sodium carbonate, 5% (w/w) Boric Acid, 5% (w/w) Sodium metasilicate, 2% (w/w) Polyvinyl alcohol)	78	[72]
Membrane support (40% (w/w) Kaolin, 15% (w/w) Quartz, 25% (w/w) Calcium carbonate, 10% (w/w) Sodium carbonate, 5% (w/w) Boric acid, 5% (w/w) Sodium metasilicate)	67	[73]
MF membrane (Wet basis: 29.63% (w/w) Kaolin, 11.11% (w/w) Quartz, 18.52% (w/w) Calcium carbonate, 7.40% (w/w) Sodium carbonate, 3.71% (w/w) Boric acid, 3.71% (w/w) Sodium metasilicate, 25.92% (w/w) Water) (Dry basis: 40% (w/w) Kaolin, 15% (w/w) Quartz, 25% (w/w) Calcium carbonate, 10% (w/w) Sodium carbonate, 5% (w/w) Boric acid, 5% (w/w) Sodium metasilicate)	130	[74]
MF membrane (92% (w/w) Soil, 4% (w/w) Sodium carbonate, 2% (w/w) Sodium metasilicate, 2% (w/w) Boric acid)	19	[75]
Composite membrane (Dry basis: 60% (w/w) Clay, 30% (w/w) Kaolin, 5% (w/w) Sodium carbonate, 2.5% (w/w) Sodium metasilicate, 2.5% (w/w) Boric acid) (Wet basis: 46.15% (w/w) Clay, 23.08% (w/w) Kaolin, 3.85% (w/w) Sodium carbonate, 1.92% (w/w) Sodium metasilicate, 1.92% (w/w) Boric acid, 23.08% (w/w) Water)	33.42	[76]
Membrane M10/25PVA (Membrane layer: 10% (w/w) Clay, 25% (w/w) Polyvinyl alcohol (12% (w/w) aqueous solution), 65% (w/w) Water Support: 85% (w/w) Clay, 15% (w/w) Wood powder, 33% (w/w) Water)	23.06	
Membrane M10 (Membrane layer: 10% (w/w) Clay, 90% (w/w) Water Support: 85% (w/w) Clay, 15% (w/w) Wood powder, 33% (w/w) Water)	21.71	In this study
Membrane M12 (Membrane layer: 12% (w/w) Clay, 88% (w/w) Water Support: 85% (w/w) Clay, 15% (w/w) Wood powder, 33% (w/w) Water)	21.60	

d_{ave}	—	Average pore diameter, μm
n	—	Number of pores considered
d_i	—	Pore diameter (μm) of i th pore
W_L	—	Weight loss, %
m_0	—	Mass of the sample before chemical contact, g
m_1	—	Mass of the sample after chemical contact, g
J	—	Permeate flux, $\text{L h}^{-1} \text{m}^{-2}$
V	—	Volume of the permeate, L
t	—	Filtration time, h
A	—	Filtering surface, m^2
UV	—	Ultra-violet spectrophotometry
CR	—	Congo Red
DWW	—	Domestic wastewater
NTU	—	Nephelometric turbidity unit
R_e	—	Turbidity elimination rate of DWW, %
NTU_f	—	Nephelometric turbidity unit of DWW in feed, 201 NTU
NTU_p	—	Nephelometric turbidity unit of DWW in permeate, NTU
SPM	—	Suspended particulate matter, mg/L
M_0	—	Mass of the empty membrane, mg
M_1	—	Mass of the membrane and the residues after drying in an oven at $105^\circ\text{C}/24\text{h}$, mg
V_w	—	Volume of filtered water, L
pH	—	Potential hydrogen
COD	—	Chemical oxygen demand, mg/L
R_d	—	Discoloration rate of CR, %
C_f	—	Concentration of CR in the feed, 0.2 g/L
C_p	—	Concentration of CR in the permeate, g/L

References

- [1] M. Benjelloun, Y. Miyah, G.A. Evrendilek, F. Zerrouq, S. Lairini, Recent advances in adsorption kinetic models: their application to dye types, *Arabian J. Chem.*, 14 (2021) 103031, doi: 10.1016/j.arabjc.2021.103031.
- [2] K. Jain, A.S. Patel, V.P. Pardhi, S.J.S. Flora, Nanotechnology in wastewater management: a new paradigm towards wastewater treatment, *Molecules*, 26 (2021) 1797, doi: 10.3390/molecules26061797.
- [3] A. Nazir, K. Khan, A. Maan, R. Zia, L. Giorno, K. Schroën, Membrane separation technology for the recovery of nutraceuticals from food industrial streams, *Trends Food Sci. Technol.*, 86 (2019) 426–438.
- [4] S. Suwal, A. Doyen, L. Bazinet, Characterization of protein, peptide and amino acid fouling on ion-exchange and filtration membranes: review of current and recently developed methods, *J. Membr. Sci.*, 496 (2015) 267–283.
- [5] W. Wen-qiong, W. Yun-chao, Z. Xiao-feng, G. Rui-xia, L. Mao-lin, Whey protein membrane processing methods and membrane fouling mechanism analysis, *Food Chem.*, 289 (2019) 468–481.
- [6] S. Zinadini, V. Vatanpour, A.A. Zinatizadeh, M. Rahimi, Z. Rahimi, M. Kian, Preparation and characterization of antifouling graphene oxide/polyethersulfone ultrafiltration membrane: application in MBR for dairy wastewater treatment, *J. Water Process Eng.*, 7 (2015) 280–294.
- [7] K. Rambabu, S. Velu, Polyethylene glycol and iron oxide nanoparticles blended polyethersulfone ultrafiltration membrane for enhanced performance in dye removal studies, *e-Polymers*, 15 (2015) 151–159.
- [8] K. Rambabu, G. Bharath, P. Monash, S. Velu, F. Banat, M. Naushad, G. Arthanareeswaran, P.L. Show, Effective treatment of dye polluted wastewater using nanoporous CaCl_2 modified polyethersulfone membrane, *Process Saf. Environ.*, 124 (2019) 266–278.
- [9] K. Rambabu, S. Velu, Improved performance of CaCl_2 incorporated polyethersulfone ultrafiltration membranes, *Period. Polytech. Chem. Eng.*, 60 (2016) 181–191.
- [10] J.L. Zhou, Sampling of Humic and Colloidal Phases in Liquid Samples, *Comprehensive Sampling and Sample Preparation*, Elsevier, 1, 2012, pp. 335–348.
- [11] N.R. Choudhury, A.G. Kannan, N.K. Dutta, Chapter 21 – Novel Nanocomposites and Hybrids for Lubricating Coating Applications, In: *Tribology and Interface Engineering Series*, Vol. 55, Elsevier, 2008, pp. 501–542.
- [12] M. Fomina, I. Skorochod, Microbial interaction with clay minerals and its environmental and biotechnological implications, *Minerals*, 10 (2020) 861, doi: 10.3390/min10100861.
- [13] M.S. Tite, I.C. Freestone, N. Wood, An investigation into the relationship between the raw materials used in the production of Chinese porcelain and stoneware bodies and the resulting microstructures, *Archaeometry*, 54 (2012) 37–55.
- [14] T. Agag, A. Akelah, Chapter 29 – Polybenzoxazine-Clay Nanocomposites, H. Ishida, T. Agag, Eds., *Handbook of Benzoxazine Resins*, Elsevier, 2011, pp. 495–516.
- [15] X. Wang, H. Wang, Structural analysis of interstratified illite-smectite by the Rietveld method, *Crystals*, 11 (2021) 244, doi: 10.3390/cryst11030244.
- [16] J.M. Huggett, *Clay Minerals*, R.C. Selley, L.R.M. Cocks, I.R. Plimer, Eds., *Encyclopedia of Geology*, Elsevier, 2005, pp. 358–365.
- [17] W. Aloulou, W. Hamza, H. Aloulou, A. Oun, S. Khemakhem, A. Jada, S. Chakraborty, S. Curcio, R.B. Amar, Developing of titania-smectite nanocomposites UF membrane over zeolite based ceramic support, *Appl. Clay Sci.*, 155 (2018) 20–29.
- [18] R. Mouratib, B. Achiou, M. El Krati, S.A. Younssi, S. Tahiri, Low-cost ceramic membrane made from alumina- and silica-rich water treatment sludge and its application to wastewater filtration, *J. Eur. Ceram. Soc.*, 40 (2020) 5942–5950.
- [19] A. Oun, N. Tahri, S.M. Chergui, B. Carbonnier, S. Majumdar, S. Sarkar, G.C. Sahoo, R. Ben Amar, Tubular ultrafiltration ceramic membrane based on titania nanoparticles immobilized on macroporous clay-alumina support: elaboration, characterization and application to dye removal, *Sep. Purif. Technol.*, 188 (2017) 126–133.
- [20] K. Suresh, G. Pugazhenth, Development of ceramic membranes from low-cost clays for the separation of oil–water emulsion, *Desal. Water Treat.*, 57 (2016) 1927–1939.
- [21] R. Chihi, I. Bliidi, M. Trabelsi-Ayadi, F. Ayari, Elaboration and characterization of a low-cost porous ceramic support from natural Tunisian bentonite clay, *C.R. Chim.*, 22 (2019) 188–197.
- [22] P. Kamgang-Syapnjeu, D. Njoya, E. Kamseu, L. Cornette de Saint Cyr, A. Marcano-Zerpa, S. Balme, M. Bechelany, L. Soussan, Elaboration of a new ceramic membrane support from Cameroonian clays, coconut husks and eggshells: application for *Escherichia coli* bacteria retention, *Appl. Clay Sci.*, 198 (2020) 105836, doi: 10.1016/j.crci.2018.12.002.
- [23] S. Khemakhem, A. Larbot, R. Ben Amar, New ceramic microfiltration membranes from Tunisian natural materials: application for the cuttlefish effluents treatment, *Ceram. Int.*, 35 (2009) 55–61.
- [24] L. Palacio, Y. Bouzerdi, M. Ouammou, A. Albizane, J. Bennazha, A. Hernández, J.I. Calvo, Ceramic membranes from Moroccan natural clay and phosphate for industrial water treatment, *Desalination*, 245 (2009) 501–507.
- [25] Y.O. Raji, M.H.D. Othman, N.A.H.S.M. Nordin, Z. ShengTai, J. Usman, S.C. Mamah, A.F. Ismail, M.A. Rahman, J. Jaafar, Fabrication of magnesium bentonite hollow fibre ceramic membrane for oil-water separation, *Arabian J. Chem.*, 13 (2020) 5996–6008.
- [26] B. Damiyine, A. Guenbour, R. Boussen, Comparative study on adsorption of cationic dye onto expanded perlite and natural clay, *Rasayan J. Chem.*, 13 (2020) 448–463.
- [27] Y. Miyah, A. Lahrichi, M. Idrissi, S. Boujraf, H. Taouda, F. Zerrouq, Assessment of adsorption kinetics for removal potential of Crystal Violet dye from aqueous solutions using

- Moroccan pyrophyllite, *J. Assoc. Arab Univ. Basic Appl. Sci.*, 23 (2017) 20–28.
- [28] Z. Bencheqroun, I. El Mrabet, M. Kachabi, M. Nawdali, I. Neves, Z. Hicham, Removal of basic dyes from aqueous solutions by adsorption onto Moroccan clay (Fez City), *Mediterr. J. Chem.*, 8 (2019) 158–167.
- [29] M. Monsif, A. Zerouale, N.I. Kandri, M. Mozzon, P. Sgarbossa, F. Zorzi, F. Tateo, S. Tamburini, E. Franceschinis, S. Carturan, R. Bertani, Chemical-physical and mineralogical characterization of ceramic raw materials from Moroccan northern regions: intriguing resources for industrial applications, *Appl. Clay Sci.*, 182 (2019) 105274, doi: 10.1016/j.clay.2019.105274.
- [30] P. Bhattacharya, S. Ghosh, A. Mukhopadhyay, Efficiency of combined ceramic microfiltration and biosorbent based treatment of high organic loading composite wastewater: an approach for agricultural reuse, *J. Environ. Chem. Eng.*, 1 (2013) 38–49.
- [31] A. Bouazizi, S. Saja, B. Achiou, M. Ouammou, J.I. Calvo, A. Aaddane, S.A. Younssi, Elaboration and characterization of a new flat ceramic MF membrane made from natural Moroccan bentonite. Application to treatment of industrial wastewater, *Appl. Clay Sci.*, 132–133 (2016) 33–40.
- [32] A. Majouli, S. Tahiri, S.A. Younssi, H. Loukili, A. Albizane, Elaboration of new tubular ceramic membrane from local Moroccan Perlite for microfiltration process. Application to treatment of industrial wastewaters, *Ceram. Int.*, 38 (2012) 4295–4303.
- [33] S. Foorginezhad, M.M. Zerafat, Microfiltration of cationic dyes using nano-clay membranes, *Ceram. Int.*, 43 (2017) 15146–15159.
- [34] A. Belgada, B. Achiou, S.A. Younssi, F.Z. Charik, M. Ouammou, J.A. Cody, K. Khaless, Low-cost ceramic microfiltration membrane made from natural phosphate for pretreatment of raw seawater for desalination, *J. Eur. Ceram. Soc.*, 41 (2021) 1613–1621.
- [35] M. Sheikhi, M. Arzani, H.R. Mahdavi, T. Mohammadi, Kaolinitic clay-based ceramic microfiltration membrane for oily wastewater treatment: assessment of coagulant addition, *Ceram. Int.*, 45 (2019) 17826–17836.
- [36] S. Velu, K. Rambabu, P. Monash, C. Sharma, Improved hydrophilic property of PES/PEG/MnCO₃ blended membranes for synthetic dye separation, *Int. J. Environ. Stud.*, 75 (2017) 592–604.
- [37] J. Rodier, B. Legube, N. Merlet, *L'analyse de l'eau*, 9th ed., Dunod, 2009.
- [38] S. Iaich, L. Messaoudi, Preparation of new ceramic supports macro-porous for microfiltration and ultrafiltration membranes based Moroccan clay, *J. Mech. Civ. Eng.*, 11 (2014) 56–62.
- [39] S. Iaich, L. Messaoudi, Mise au point et caractérisation des membranes minérales de micro-filtration déposées sur des supports céramiques tubulaires à base d'une argile Marocaine naturelle, *J. Mater. Environ. Sci.*, 5 (2014) 1808–1815.
- [40] L. Bouna, Ph.D. Thesis, Université de Toulouse, France, 2012.
- [41] O. Qabaqous, N. Tijani, M.N. Bennani, A.E. Krouk, Elaboration et caractérisation des supports plans à base d'argile (Rhassoul) pour membranes minérales, *J. Mater. Environ. Sci.*, 5 (2014) 2244–2249.
- [42] P.B. Arab, T.P. Araújo, O.J. Pejon, Identification of clay minerals in mixtures subjected to differential thermal and thermogravimetry analyses and methylene blue adsorption tests, *Appl. Clay Sci.*, 114 (2015) 133–140.
- [43] F.G.M. Aredes, T.M.B. Campos, J.P.B. Machado, K.K. Sakane, G.P. Thim, D.D. Brunelli, Effect of cure temperature on the formation of metakaolinite-based geopolymer, *Ceram. Int.*, 41 (2015) 7302–7311.
- [44] P. Ptáček, F. Frajkorová, F. Šoukal, T. Opravil, Kinetics and mechanism of three stages of thermal transformation of kaolinite to metakaolinite, *Powder Technol.*, 264 (2014) 439–445.
- [45] A.I. Ivanets, T.A. Azarova, V.E. Agabekov, S.M. Azarov, Ch. Batsukh, D. Batsuren, V.G. Prozorovich, A.A. Rat'ko, Effect of phase composition of natural quartz raw material on characterization of microfiltration ceramic membranes, *Ceram. Int.*, 42 (2016) 16571–16578.
- [46] L. Morales, E. Garzón, E. Romero, P.J. Sánchez-Soto, Microbiological induced carbonate (CaCO₃) precipitation using clay phyllites to replace chemical stabilizers (cement or lime), *Appl. Clay Sci.*, 174 (2019) 15–28.
- [47] J. Bentama, K. Ouazzani, P. Schmitz, Mineral membranes made of sintered clay: application to crossflow microfiltration, *Desalination*, 146 (2002) 57–61.
- [48] J.W. Chew, J. Kilduff, G. Belfort, The behavior of suspensions and macromolecular solutions in crossflow microfiltration: an update, *J. Membr. Sci.*, 601 (2020) 117865, doi: 10.1016/j.memsci.2020.117865.
- [49] R. Antonelli, G.R.P. Malpass, M.G.C. da Silva, M.G.A. Vieira, Adsorption of ciprofloxacin onto thermally modified bentonite clay: experimental design, characterization, and adsorbent regeneration, *J. Environ. Chem. Eng.*, 8 (2020) 104553, doi: 10.1016/j.jece.2020.104553.
- [50] G.O. Ihekwe, J.N. Shondo, K.I. Orisekeh, M.K.-U. Godwin, C.N. Iheoma, P.O. Azikiwe, Characterization of certain Nigerian clay minerals for water purification and other industrial applications, *Heliyon*, 6 (2020) e03783, doi: 10.1016/j.heliyon.2020.e03783.
- [51] Y. Miyah, A. Lahrichi, R. Kachkoul, G. El Mouhri, M. Idrissi, S. Iaich, F. Zerrouq, Multi-parametric filtration effect of the dyes mixture removal with the low cost materials, *Arab J. Basic Appl. Sci.*, 27 (2020) 248–258.
- [52] R.L. Frost, The dehydroxylation of the kaolinite clay minerals using infrared emission spectroscopy, *Clays Clay Miner.*, 44 (1996) 635–651.
- [53] M. Hajjaji, Mineralogy and thermal transformation of clayey materials from the district of Marrakech, Morocco, *Commun. Geol.*, 101 (2014) 75–80.
- [54] A. Majouli, S.A. Younssi, S. Tahiri, A. Albizane, H. Loukili, M. Belhaj, Characterization of flat membrane support elaborated from local Moroccan Perlite, *Desalination*, 277 (2011) 61–66.
- [55] M.A. Moghadam, R.A. Izadifard, Effects of zeolite and silica fume substitution on the microstructure and mechanical properties of mortar at high temperatures, *Constr. Build. Mater.*, 253 (2020) 119206, doi: 10.1016/j.conbuildmat.2020.119206.
- [56] K. Lazdovica, L. Liepina, V. Kampars, Catalytic pyrolysis of wheat bran for hydrocarbons production in the presence of zeolites and noble-metals by using TGA-FTIR method, *Bioresour. Technol.*, 207 (2016) 126–133.
- [57] Y.-F. Chen, M.-C. Wang, M.-H. Hon, Phase transformation and growth of mullite in kaolin ceramics, *J. Eur. Ceram. Soc.*, 24 (2004) 2389–2397.
- [58] L. Zerbo, Ph.D. Thesis, Université de Ouagadougou, Burkina Faso, 2009.
- [59] B. Ghouil, A. Harabi, F. Bouzerara, B. Boudaira, A. Guechi, M.M. Demir, A. Figoli, Development and characterization of tubular composite ceramic membranes using natural aluminosilicates for microfiltration applications, *Mater. Charact.*, 103 (2015) 18–27.
- [60] J. Saikia, S. Sarmah, J.J. Bora, B. Das, R.L. Goswamee, Preparation and characterization of low cost flat ceramic membranes from easily available potters' clay for dye separation, *Bull. Mater. Sci.*, 42 (2019) 1–13.
- [61] H.M. Yeh, T.W. Cheng, J.W. Tsai, Modified concentration polarization model for hollow-fiber membrane ultrafiltration, *Sep. Purif. Technol.*, 16 (1999) 189–192.
- [62] P.B. Belibi, M.M.G. Nguemtchouin, M. Rivallin, J.N. Nsami, J. Sieliechi, S. Cerneaux, M.B. Ngassoum, M. Cretin, Microfiltration ceramic membranes from local Cameroonian clay applicable to water treatment, *Ceram. Int.*, 41 (2015) 2752–2759.
- [63] M. Mouiya, A. Abourriche, A. Bouazizi, A. Benhammou, Y. El Hafiane, Y. Abouliatim, L. Nibou, M. Oumam, M. Ouammou, A. Smith, H. Hannache, Flat ceramic microfiltration membrane based on natural clay and Moroccan phosphate for desalination and industrial wastewater treatment, *Desalination*, 427 (2018) 42–50.
- [64] S. Khemakhem, R.B. Amar, Grafting of fluoroalkylsilanes on characterization Tunisian clay membrane, *Ceram. Int.*, 37 (2011) 3323–3328.
- [65] A. Agarwal, A. Samanta, B.K. Nandi, A. Mandal, Synthesis, characterization and performance studies of kaolin-fly ash-based

- membranes for microfiltration of oily waste water, *J. Petrol. Sci. Eng.*, 194 (2020) 107475, doi: 10.1016/j.petrol.2020.107475.
- [66] B. Achiou, H. Elomari, A. Bouazizi, A. Karim, M. Ouammou, A. Albizane, J. Bennazha, S.A. Younssi, I.E. El Amrani, Manufacturing of tubular ceramic microfiltration membrane based on natural pozzolan for pretreatment of seawater desalination, *Desalination*, 419 (2017) 181–187.
- [67] N. Malik, V.K. Bulasara, S. Basu, Preparation of novel porous ceramic microfiltration membranes from fly ash, kaolin and dolomite mixtures, *Ceram. Int.*, 46 (2020) 6889–6898.
- [68] N.C. Homem, N. de Camargo Lima Beluci, S. Amorim, R. Reis, A.M.S. Vieira, M.F. Vieira, R. Bergamasco, M.T.P. Amorim, Surface modification of a polyethersulfone microfiltration membrane with graphene oxide for reactive dyes removal, *Appl. Surf. Sci.*, 486 (2019) 499–507.
- [69] B.D. Bhide, S.A. Stern, A new evaluation of membrane processes enrichment of air. II. Effects of economic membrane properties, *J. Membr. Sci.*, 62 (1991) 37–58.
- [70] W.J. Koros, R. Mahajan, Pushing the limits on possibilities for large scale gas separation: which strategies?, *J. Membr. Sci.*, 175 (2000) 181–196.
- [71] D. Vasanth, G. Pugazhenth, R. Uppaluri, Performance of low cost ceramic microfiltration membranes for the treatment of oil-in-water emulsions, *Sep. Sci. Technol.*, 48 (2013) 849–858.
- [72] S. Emani, R. Uppaluri, M.K. Purkait, Preparation and characterization of low cost ceramic membranes for mosambi juice clarification, *Desalination*, 317 (2013) 32–40.
- [73] D. Vasanth, R. Uppaluri, G. Pugazhenth, Influence of sintering temperature on the properties of porous ceramic support prepared by uniaxial dry compaction method using low-cost raw materials for membrane applications, *Sep. Sci. Technol.*, 46 (2011) 1241–1249.
- [74] B.K. Nandi, R. Uppaluri, M.K. Purkait, Identification of optimal membrane morphological parameters during microfiltration of mosambi juice using low cost ceramic membranes, *LWT – Food Sci. Technol.*, 44 (2011) 214–223.
- [75] S. Jana, M.K. Purkait, K. Mohanty, Preparation and characterization of low-cost ceramic microfiltration membranes for the removal of chromate from aqueous solutions, *Appl. Clay Sci.*, 47 (2010) 317–324.
- [76] P. Mittal, S. Jana, K. Mohanty, Synthesis of low-cost hydrophilic ceramic-polymeric composite membrane for treatment of oily wastewater, *Desalination*, 282 (2011) 54–62.